Journal of Applied Mathematics and Computing (2024) 70:3441–3476
https://doi.org/10.1007/s12190-024-02105-4

ORIGINAL RESEARCH

Stability and complex dynamical analysis of COVID-19 epidemic model with non-singular kernel of Mittag-Leffler law

Saba Jamil[1] · Parvaiz Ahmad Naik[2] · Muhammad Farman[3,4] · Muhammad Umer Saleem[5] · Abdul Hamid Ganie[6]

Received: 21 March 2024 / Revised: 21 April 2024 / Accepted: 23 April 2024 /
Published online: 7 May 2024

Abstract
One of the global problems and a number of societal challenges in the areas of social life, the economy, and international communications is COVID-19. In order to counteract the impact of sickness on society, we created a deterministic COVID-19 model in this study that uses real data to assess the impact of disease, dynamical transmission, quarantine impact, and hospitalized treatment. The model includes a generalized form of the fractal and fractional operator. This study aims to develop a fractal-fractional mathematical model suitable for the lifestyle of the Thai population facing the COVID-19 situation. The model divides the incubation period into the quarantine class and the exposed class, which later moved to the hospitalized infected class and the infected class. The fractal-fractional derivative is used to analyze the dynamics of the population in these classes, providing a more detailed understanding of the epidemic's progression and the effectiveness of control measures. The existence and uniqueness of the solution were also determined with the Lipschitz condition and fixed point theory. With the use of simulations and functional analysis tools like Ulam-Hyers, we examine the sensitivity analysis of the fractal-fractional model with respect to each parameter effect. We develop a numerical scheme for the fractal-fractional model

✉ Parvaiz Ahmad Naik
naik.parvaiz@ymun.edu.cn

1 Institute of Mathematics, Khawaja Fareed University of Engineering and Information Technology, Rahim Yar Khan, Pakistan

2 Department of Mathematics and Computer Science, Youjiang Medical University for Nationalities, Baise 533000, Guangxi, China

3 Faculty of Arts and Sciences, Department of Mathematics, Near East University, Mersin, Turkey

4 Department of Computer Science and Mathematics, Lebanese American University, Beirut, Lebanon

5 Department of Mathematics, University of Education, Lahore, Pakistan

6 Department of Basic Science, College of Science and Theoretical Studies, Saudi Electronic University, Riyadh, Saudi Arabia

based on Newton polynomial for computational analysis and convergence solution to steady-state points of real data COVID-19 in Thailand. The verification of the examined fractional-order model with actual COVID-19 data for Thailand demonstrates the potential of the suggested paradigm in forecasting and comprehending the dynamics of the pandemic. Furthermore, the fractal fractional-order derivative gives rise to a range of chaotic behaviors that show how the species has changed over place and time. Fractional-order epidemiological models may help predict and understand the course of the COVID-19 pandemic and provide relevant management approaches.

Keywords COVID-19 Model · Mittage-Leffler Kernel · Fractal-fractional derivative · Existence and uniqueness · Ulam-Hyers Stability · Newton polynomial interpolation

1 Introduction

Coronavirus is one of the major health issues that started in 2019 in China and affects the globe all over the world [1]. After this virus quickly spread from person to person and to many different nations, the World Health Organisation (WHO) declared a global health emergency in late January 2020 [2, 3] as a result of the sharp rise in the number of afflicted persons. Medical requirements, as well as the number of medical workers, were therefore insufficient to deal with the rising number of infected individuals [4]. Many nations are concerned about the spread of this virus and are scrambling to develop solutions to help the rising patient population reduce death. The WHO reported on 8 December 2022 that there had been over 6,625,029 fatalities and 642,924,560 cases overall. There were 33,285 fatalities and 4,711,528 total cases in Thailand [5]. If we are unable to control this virus, it is projected that the number of infections and fatalities will surely rise in the future. A mathematical model is one of the intriguing methods for analyzing the epidemic scenario. The use of mathematical models to represent natural problems is important to understanding real-life issues in different fields. Mathematical models can be used to predict future outbreaks in this situation. The outcome will serve as a guide for creating epidemic prevention and eradication strategies [6, 7]. For instance, how many people are becoming infected on the rise, and how can this tendency be stopped so that fewer people die and each nation finds an appropriate solution? The model helps establish the best approaches to control the pandemic since it provides direction for doing so. Mathematical models, which are amorphous structures, are used to describe and construct behavioral systems [6, 7]. Real-world situations are converted into problems that closely resemble them using mathematical tools, which are then mathematically solved and evaluated to predict outcomes in those scenarios [8–13]. The source [14] delves into the numerical treatment of delay differential equations and their applications in bioscience.

Numerous fractional and fractal mathematical models of COVID-19 have also been developed by scholars in recent years. We will now briefly review a few studies on the COVID-19. In reference [15], optimal control problems are addressed utilizing the Atangana-Baleanu fractional derivative. The authors Kolabje et al. [16] examined the development of the time series for the overall number of confirmed cases of

COVID-19, a novel coronavirus illness, for several African countries and the application of fractional-order derivative for the COVID-19 model also studied in [17–21]. For the investigation and dynamical transmission of the virus, writers in [22] presented the COVID-19 omicron variant model using the Caputo-Fabrizio operator. Fractional modeling, optimal control strategies for mutated COVID-19 pandemic [23]. Study [24] explores theoretical and numerical aspects of solutions via simulations for a fractal-fractional waterborne disease model. In [25] investigates the Ulam stability of fractional differential equations with a fractional Caputo-type derivative using the fractional Fourier transform. In [26] study presents an HIV/AIDS epidemic model incorporating fractional-order dynamics with a Mittag-Leffler kernel. The fractional-order model was generalized using the Laplace transform to ensure stability and a unique solution for the iterative strategy. In the context of the Caputo operator. The study of the second wave of the coronavirus in India was the primary focus of the paper [27]. Multi-model selection and analysis for COVID-19 include two-sided fractional modeling qualitatively and quantitatively [28, 29]. The COVID-19 model, which is a set of fractional differential equations with illness effects, was developed by researchers. The article [30] provides a detailed analysis of COVID-19 stochastic modeling incorporating different transmission rates and simulations based on real statistical data from multiple countries. Some other applications of the fractional operator in BAM neural network, delay in a chemical reaction and predator pray system studied in [31]. Memory effects, hereditary characteristics, and non-local behaviors can all be included with fractional calculus, which is essential for faithfully simulating real-world events such as the dynamics of disease transmission. Furthermore, temporal delays play a critical role in capturing the delayed responses found in biological systems, which leads to a more accurate depiction of the related dynamics. The study [32], explores the dynamics of a fractional-order asymptomatic COVID-19 model with multiple time-delays, focusing on stability and bifurcation analysis to understand the behavior of the model under various conditions. The research [33], investigates the dynamics and sensitivity of a fractional-order delay differential model for COVID-19 infection. The impact on mucus fluid due to the surge of the pandemic COVID-19 was scrutinized by Padmavathi et al. [34]. Additionally, innovative mathematical models were introduced to characterize the novel coronavirus [35, 36].

The paper's innovation lies in employing a non-singular kernel derived from the Mittag-Leffler law within the framework of fractal fractional derivatives. This method enhances the accuracy of modeling COVID-19 spread by capturing the system's memory and hereditary properties. While previous research has explored the use of non-singular kernels from the Mittag-Leffler law in fractional derivatives, the application of fractal fractional operators, especially in understanding COVID-19 dynamics, remains limited. Thus, this paper offers a significant contribution to COVID-19 modeling by introducing a fresh approach to model disease spread and conducting a stability analysis of the proposed model. Inspired by the previously mentioned research and the pressing need to determine the best course of action for handling the COVID-19 pandemic, this study aims to investigate a fractal fractional-order model to better understand the complexities of COVID-19 infections and evaluate the effectiveness of different control strategies, particularly quarantine, that are put into place inside the borders of Thailand. This research aims to close this gap, in contrast to current COVID-19 models that frequently ignore the influence of control measures like quarantine and their effects on different demographic groups. The model improves the prediction of COVID-19 dissemination and offers a tactical framework for taking proactive steps to lessen its effects by factoring in the efficacy of quarantine measures. This model stands out due to its distinctive approach, which provides insights into customized interventions and tactics to effectively combat the epidemic in Thailand. This study is divided into the following sections: the proposed model is introduced in detail in Sect. 1, and Sect. 2 addresses numerous fundamental fractional-order derivatives that help solve the epidemiological model. In Sect. 3, the model is generalized, and the description of the suggested model is analyzed. Section 4 examines the suggested model's sensitivity analysis. Existence and uniqueness are verified in Sect. 5. Ulam-Hyers Stability is analyzed in Sect. 6. Section 7 examines the numerical technique of the Mittag-Leffler kernel. Sections 8 and 9, respectively, discuss numerical simulations and the outcome of the study as concluding remarks.

2 Preliminaries

Here, we give a few key definitions that might be useful to analyze the model.

Definition 2.1 [7] Assume that $\Phi(t)$ represent a function that is not necessarily differentiable. Let the fractal dimension (η) and the fractional-order (υ_1) be the corresponding variables. Then for $0 < \upsilon_1, \eta \leq 1$, the fractal-fractional derivative of order υ_1 in the Riemann-Liouville terms:

- That has a power law kernel is provided as:

$$ {}_{0}^{FFP}D_t^{\upsilon_1,\eta}\Phi(t) = \frac{1}{\Gamma(n-\upsilon_1)}\frac{d^n}{dt^n}\int_0^t (t-\zeta)^{n-\upsilon_1-1}\Phi(\zeta)d\zeta, \tag{1} $$

  where $n-1 < \upsilon_1, \eta < n \in \mathbb{N}$. And

$$ \frac{D\Phi(\zeta)}{D\zeta^\eta} = \lim_{t\to\zeta}\frac{\Phi(t)-\Phi(\zeta)}{t^\eta-\zeta^\eta}. \tag{2} $$

- With an exponential decay kernel is expressed as:

$$ {}_{0}^{FFE}D_t^{\upsilon_1,\eta}\Phi(t) = \frac{M(\upsilon_1)}{\Gamma(n-\upsilon_1)}\frac{d^n}{dt^n}\int_0^t \exp\Big[-\frac{\upsilon_1}{1-\upsilon_1}(t-\zeta)\Big]\Phi(\zeta)d\zeta. \tag{3} $$

- As follows when using the Mittag-Leffler kernel:

$$ {}_{0}^{FFM}D_t^{\upsilon_1,\eta}\Phi(t) = \frac{AB(\upsilon_1)}{1-\upsilon_1}\frac{d^n}{dt^n}\int_0^t \Phi(\zeta)E_{\upsilon_1}\Big[-\frac{\upsilon_1}{1-\upsilon_1}(t-\zeta)_1^{\upsilon}\Big]d\zeta. \tag{4} $$

Definition 2.2 [7] Let $\Phi(t)$ be continuous on (a,b) and $0 < \upsilon_1, \eta \leq 1$, then the fractal-fractional integral of $\Phi(t)$ with fractional-order υ_1 and fractal-order η:

- With a power law kernel is defined as:

$$ {}_0^{FFP}I^{\upsilon_1,\eta}\Phi(t) = \frac{1}{\Gamma(\upsilon_1)}\int_0^t (t-\zeta)^{\upsilon_1-1}\zeta^{1-\eta}\Phi(\zeta)d\zeta. \tag{5} $$

- With an exponential decay kernel is defined as:

$$ {}_0^{FFE}I^{\upsilon_1,\eta}\Phi(t) = \frac{\eta(1-\upsilon_1)t^{\eta-1}\Phi(t)}{M(\upsilon_1)} + \frac{\upsilon_1\eta}{M(\upsilon_1)}\int_0^t \zeta^{\upsilon_1-1}\Phi(\zeta)d\zeta. \tag{6} $$

- With the Mittag-Leffler kernel is defined as:

$$ \begin{aligned} {}_0^{FFM}I^{\upsilon_1,\eta}\Phi(t) &= \frac{\eta(1-\upsilon_1)t^{\eta-1}\Phi(t)}{AB(\upsilon_1)} \\ &\quad + \frac{\upsilon_1\eta}{AB(\upsilon_1)\Gamma(\upsilon_1)}\int_0^t (t-\zeta)^{\upsilon_1-1}\zeta^{\eta-1}\Phi(\zeta)d\zeta. \end{aligned} \tag{7} $$

3 COVID-19 Fractional-Order Model

The integration of the fractal-fractional operator has been applied to enhance the modeling of the COVID-19 pandemic, as it enables the representation of intricate dynamics, memory effects, and non-local behaviors inherent in epidemic processes. By incorporating this operator, the model can better capture the complex interactions and temporal dependencies seen in the transmission of diseases like COVID-19. This approach offers a more thorough framework for studying epidemic dynamics, enhancing predictive precision, and offering valuable insights for devising effective control measures and preventive strategies. We consider COVID-19 in Thailand classical model which is given in [8], having seven compartments such as susceptible population (S), quarantine population (Q), exposed class E, hospitalized infected population I_h infected population (I), recovered population (R), and pathogens population (P). We now use a generalized form of fractal-fractional with mittag-leffler kernels to reform this model into a fractional-order to track the impact of this virus on society and the spread of dynamic forces. Initially, the susceptible class should be considered a disease-free, healthy population. The susceptible class enters the incubation phase when they are exposed to an infected population or to pathogens that are dispersed throughout an infected population and into the environment. The fact that the natural birth and death rates of the population affect the population dynamics in the sensitive class is another unavoidable element. Second, take into account the population during the incubation period, which is separated into two classes: exposed classes and quarantine classes. The exposed classes and quarantine classes represent the populations that were, respectively, not and were in quarantine during the incubation period. Following this, the exposed classes and quarantine classes become hospitalized infected and infected classes, though some exposure classes may need to be hospitalized if their symptoms are severe. Additionally, take into account that the population of exposed classes and quarantined classes has decreased as a result of natural mortality. Third, take into account the dynamics of the afflicted population, which includes both the afflicted classes and the hospitalized sick. After the incubation time, the rise in both classes becomes the infected class, which is then transformed into the recovered class. Both natural mortality and COVID-19-related mortality correspond with population dynamics in the hospitalized infected and infected classes. Furthermore, the contaminated group can disperse the viruses throughout the surroundings. The population's ability to recover in the affected class then determines how much of the recovered class is recovered. This group enters the susceptible class if there is a lack of immunity. Permanent immunity cannot be achieved following COVID-19 recovery. Lastly, the pathogens class part determines the rise in pathogens in the environment due to the infected class's coughing or sneezing. There is a natural mortality rate for the pathogens. We have the following system of fractal fractional-order equations

$$\begin{aligned}
&{}^{FFM}D_{0,t}^{\upsilon,\varsigma} S(t) = A^{\upsilon} + m^{\upsilon} R - \tfrac{\alpha^{\upsilon} SP}{1+\omega_1^{\upsilon} P} - \tfrac{\beta^{\upsilon} S(I+I_h)}{1+\omega_2^{\upsilon}(I+I_h)} - \kappa^{\upsilon} S,\\
&{}^{FFM}D_{0,t}^{\upsilon,\varsigma} Q(t) = \tfrac{\alpha^{\upsilon} SP}{1+\omega_1^{\upsilon} P} + \tfrac{\beta S(I+I_h)}{1+\omega_2^{\upsilon}(I+I_h)} - \gamma_1^{\upsilon} Q - \kappa^{\upsilon} Q,\\
&{}^{FFM}D_{0,t}^{\upsilon,\varsigma} E(t) = \tfrac{(1-\sigma^{\upsilon})\alpha^{\upsilon} SP}{1+\omega_1^{\upsilon} P} + \tfrac{(1-\sigma^{\upsilon})\beta^{\upsilon} S(I+I_h)}{1+\omega_2^{\upsilon}(I+I_h)} - \theta^{\upsilon}\gamma_2^{\upsilon} E - (1-\sigma^{\upsilon})\theta^{\upsilon}\gamma_2^{\upsilon} E - \kappa^{\upsilon} E,\\
&{}^{FFM}D_{0,t}^{\upsilon,\varsigma} I_h(t) = \gamma_1^{\upsilon} Q + (1-\theta^{\upsilon})\gamma_2^{\upsilon} E - \eta_1^{\upsilon} I_h - (\kappa^{\upsilon} + \delta^{\upsilon}) I_h,\\
&{}^{FFM}D_{0,t}^{\upsilon,\eta} I(t) = \theta^{\upsilon}\gamma_2^{\upsilon} E - \eta_2^{\upsilon} I - (\kappa^{\upsilon} + \delta^{\upsilon}) I,\\
&{}^{FFM}D_{0,t}^{\upsilon,\varsigma} R(t) = \eta_1^{\upsilon} I_h + \eta_2^{\upsilon} I - m^{\upsilon} R - \kappa^{\upsilon} R,\\
&{}^{FFM}D_{0,t}^{\upsilon,\varsigma} P(t) = \mu^{\upsilon} I - \kappa_p^{\upsilon} P,
\end{aligned} \tag{8}$$

with initial conditions lying in a positive region,

$$S(0) \geq 0, \quad Q(0) \geq 0, \quad E(0) \geq 0, \quad I_h(0) \geq 0, \quad I(0) \geq 0, \quad R(0) \geq 0, \quad P(0) \geq 0.$$

In this model, various parameters are defined to characterize different aspects of a population's dynamics within the context of infectious disease transmission. A^{υ} represents the birth rate of the human population, while κ^{υ} signifies the natural human death rate. σ^{υ} denotes the probability of the susceptible population being quarantined, and θ^{υ} indicates the probability of transitioning from being exposed to being infected. The parameters α^{υ} and β^{υ} govern the rates of pathogen-induced transfer from susceptible to exposed classes and the spread of infection from susceptible to exposed classes due to infected individuals, respectively. ω_1^{υ} and ω_2^{υ} represent the percentages of contact with an infectious environment and with infected individuals, respectively. γ_1^{υ} and γ_2^{υ} characterize the rates of transition from quarantine to the hospitalized class and from the exposed class to the infected class, respectively. η_1^{υ} and η_2^{υ} signify the recovery rates of hospitalized infected populations and the overall diseased population, respectively. δ^{υ} denotes the coronavirus mortality rate, while μ^{υ} represents the rate of virus transmission to the environment by class of infection. κ_p^{υ} signifies the pathogen mortality rate due to natural causes. Finally, m^{υ} describes the rate at which an individual who has recovered transitions back into the susceptible class.

4 Analysis of Model

4.1 Equilibrium Points Analysis

The two distinct kinds of equilibrium points are endemic equilibrium points and disease-free equilibrium points. To discover them, the right-hand sides of the system (8) equations are set to zero. The disease-free equilibrium points $\mathbb{E}^0$ are:

$$K^0 = (S^0, Q^0, E^0, I_h^0, R^0, P^0) = (\frac{A^\upsilon}{\kappa^\upsilon}, 0, 0, 0, 0, 0, 0). \tag{9}$$

The endemic equilibrium points are $\mathbb{E}^\circ = (S^\circ, Q^\circ, E^\circ, I_h^\circ, R^\circ, P^\circ)$,

$$\begin{aligned}
S^\circ &= \frac{A^\upsilon}{\kappa^\upsilon} + \frac{m^\upsilon}{\kappa^\upsilon} R^\circ - \frac{\gamma_1^\upsilon + \kappa^\upsilon}{\kappa^\upsilon} Q^\circ, \\
Q^\circ &= \frac{\eta_1^\upsilon + \kappa^\upsilon + \delta^\upsilon}{\gamma_1} I_h^\circ - \frac{(1-\theta^\upsilon)}{\gamma_1^\upsilon} E^\circ, \\
E^\circ &= \frac{\eta_2^\upsilon + \kappa^\upsilon + \delta^\upsilon}{\theta^\upsilon \gamma_2^\upsilon} I^\circ, \\
I_h^\circ &= \frac{A^\upsilon - \kappa^\upsilon N^\circ}{\delta^\upsilon} - I^\circ, \\
I^\circ &= \frac{-B_2 + \sqrt{B_2^2 - 4B_1B_3}}{2B_1}, \\
R^\circ &= \frac{\eta_1^\upsilon I_h^\circ + \eta_2^\upsilon I^\circ}{m^\upsilon + \kappa^\upsilon}, \\
P^\circ &= \frac{\mu^\upsilon I^\circ}{\kappa_p^\upsilon},
\end{aligned} \tag{10}$$

where

$$\begin{aligned}
B_1 &= ((1-\sigma^\upsilon)\alpha^\upsilon \mu + x_1 \omega_1^\upsilon \mu^\upsilon)(x_3 - x_2) - x_4 \omega_1^\upsilon \mu^\upsilon, \\
B_2 &= ((1-\sigma^\upsilon)\alpha^\upsilon \mu + x_1 \omega_1^\upsilon \mu^\upsilon)\left(A^\upsilon + x_2\left(\frac{A^\upsilon - \kappa^\upsilon N^\circ}{\delta}\right)\right) \\
&\quad - x_1 \kappa_p^\upsilon (x_3 - x_2) - x_4 \kappa_p^\upsilon, \\
B_3 &= x_1 \kappa_p^\upsilon \left(A^\upsilon + x_2\left(\frac{A^\upsilon - \kappa^\upsilon N^\circ}{\delta^\upsilon}\right)\right),
\end{aligned}$$

with

$$\begin{aligned}
x_1 &= \frac{(1-\sigma^\upsilon)\beta^\upsilon(A^\upsilon - \kappa^\upsilon N^\circ)}{\delta^\upsilon + \omega_2^\upsilon(A - \kappa^\upsilon N^\circ)}, x_2 = \frac{m^\upsilon \eta_1^\upsilon}{m^\upsilon + \kappa^\upsilon} - \frac{(\gamma_1^\upsilon + \kappa^\upsilon)(\eta_1^\upsilon + \kappa^\upsilon + \delta^\upsilon)}{\gamma_1^\upsilon}, \\
x_3 &= \frac{m^\upsilon \eta_2^\upsilon}{m^\upsilon + \kappa^\upsilon} - \frac{\eta_1^\upsilon + \kappa^\upsilon + \delta^\upsilon}{\theta^\upsilon \gamma_2^\upsilon}\left(\frac{(1-\theta^\upsilon)\gamma_2^\upsilon(\gamma_1^\upsilon + \kappa^\upsilon)}{\gamma_1^\upsilon} - (\gamma_2^\upsilon + \kappa^\upsilon)\right),
\end{aligned}$$

Table 1 Sensitivity indices of $\mathscr{R}_0$ parameters

Parameter	Index	Parameter	Index
σ^{υ}	+0.0072	κ^{υ}	−1.0003
β^{υ}	+1.0000	η_1^{υ}	0.1788
A^{υ}	+1.0000	η_2^{υ}	−0.7269
θ^{υ}	−0.1752	δ^{υ}	−0.00093886
γ_1^{υ}	+0.0000050941	μ^{υ}	+0.0052
γ_2^{υ}	+0.00010409	κ_p^{υ}	−0.0052

$$x_4 = \frac{\kappa^{\upsilon}(\gamma_2^{\upsilon} + \kappa^{\upsilon})(\eta_2^{\upsilon} + \kappa^{\upsilon} + \delta^{\upsilon})}{\theta^{\upsilon}\gamma_2^{\upsilon}}.$$

The basic reproductive number "$\mathscr{R}_0''$ given in [8] is:

$$\mathscr{R}_0 = \frac{(1-\sigma^{\upsilon})\beta^{\upsilon}A^{\upsilon}(1-\theta^{\upsilon})\gamma_2^{\upsilon}}{\kappa^{\upsilon}y_2y_3} + \frac{(1-\sigma^{\upsilon})\beta^{\upsilon}A^{\upsilon}\theta^{\upsilon}\gamma_2^{\upsilon}}{\kappa^{\upsilon}y_2y_4} + \frac{(1-\sigma^{\upsilon})\alpha^{\upsilon}A^{\upsilon}\theta^{\upsilon}\gamma_2^{\upsilon}\mu^{\upsilon}}{\kappa^{\upsilon}y_2y_4\kappa_p^{\upsilon}} + \frac{\sigma^{\upsilon}\beta^{\upsilon}A^{\upsilon}\gamma_1}{\kappa^{\upsilon}y_1y_3}, \tag{11}$$

where $y_1 = \gamma_1^{\upsilon} + \kappa^{\upsilon}$, $y_2 = \gamma_2^{\upsilon} + \kappa^{\upsilon}$, $y_3 = \eta_1^{\upsilon} + \kappa^{\upsilon} + \delta^{\upsilon}$ and $y_4 = \eta_2^{\upsilon} + \kappa^{\upsilon} + \delta^{\upsilon}$.

4.2 Sensitivity Analysis

Sensitivity analysis is a method used to determine how changes or uncertainties in model input affect the uncertainties in model output, thus gauging the extent to which different sources of uncertainty impact the final results. By considering the importance of each parameter in the disease dynamics, it is possible to reduce or handle the occurrence and prevalence of COVID-19. Investigated in this case is how each parameter affects the fundamental reproduction number $\mathscr{R}_0$. The infection rate's sensitivity index β^{υ} is calculated using the normalized forward sensitivity index technique (NFSIM).

$$\sum_{\beta^{\upsilon}}^{\mathscr{R}_0} = \frac{\partial R_0}{\partial \beta^{\upsilon}} \times \frac{\beta^{\upsilon}}{\mathscr{R}_0},$$
$$\sum_{\beta^{\upsilon}}^{\mathscr{R}_0} = 0.9948 \approx 1.0000. \tag{12}$$

Consequently, the infection rate's sensitivity index is $\beta^{\upsilon} = 1.0000$. Similar calculations and tabulations are made for the remaining sensitivity indices in Table 1.

The metrics exhibiting a positive sensitivity index demonstrate the beneficial relevance of the increase in the fundamental reproductive numbers. Consequently, adjustments to the parameter's value while maintaining the same values for the other parameters will have an impact on modifications to the basic reproductive statistics. A parameter with a negative sensitivity index signifies that there is a negative importance to the increase in fundamental reproductive numbers. On the one hand, the factor that most inhibits the spread of the illness is the percentage of the natural human death rate. Because $\sum_{\beta^{\upsilon}}^{\mathscr{R}_0} = 0.9948$, a 10% increase (or decrease) in the parameter β^{υ} will cause a 9.948% increase (or reduction) in the value $\mathscr{R}_0$. The finding of $\sum_{\kappa^{\upsilon}}^{\mathscr{R}_0} = -1.0003$ means that a 10% increase (or decrease) in the parameter κ^{υ} will cause a 10.003% decrease (or increase) in the value of $\mathscr{R}_0$.

5 Proposed Model's Existence and Uniqueness

In this section, we will demonstrate the theorem that establishes the existence and uniqueness of solutions for the proposed model (8). We verify the existence of the fractal-fractional model (8) using the fixed point method.

$$
\begin{aligned}
S(t)-S(0) &= \frac{\varsigma(1-\upsilon)t^{\varsigma-1}}{AB(\upsilon)}\mathrm{H}_1(t,S)+\frac{\upsilon\varsigma}{\mathscr{A}\mathscr{B}(\upsilon)\Gamma(\upsilon)}\int_0^t (t-\zeta)^{\upsilon-1}\zeta^{\varsigma-1}\mathrm{H}_1(\varsigma,S)d\zeta,\\
Q(t)-Q(0) &= \frac{\varsigma(1-\upsilon)t^{\varsigma-1}}{\mathscr{A}\mathscr{B}(\upsilon)}\mathrm{H}_2(t,Q)+\frac{\upsilon\varsigma}{\mathscr{A}\mathscr{B}(\upsilon)\Gamma(\upsilon)}\int_0^t (t-\zeta)^{\upsilon-1}\zeta^{\varsigma-1}\mathrm{H}_2(\varsigma,Q)d\zeta,\\
E(t)-E(0) &= \frac{\varsigma(1-\upsilon)t^{\varsigma-1}}{\mathscr{A}\mathscr{B}(\upsilon)}\mathrm{H}_3(t,E)+\frac{\upsilon\varsigma}{\mathscr{A}\mathscr{B}(\upsilon)\Gamma(\upsilon)}\int_0^t (t-\zeta)^{\upsilon-1}\zeta^{\varsigma-1}\mathrm{H}_3(\varsigma,E)d\zeta,\\
I_h(t)-I_h(0) &= \frac{\varsigma(1-\upsilon)t^{\varsigma-1}}{\mathscr{A}\mathscr{B}(\upsilon)}\mathrm{H}_4(t,I_h)+\frac{\upsilon\varsigma}{\mathscr{A}\mathscr{B}(\upsilon)\Gamma(\upsilon)}\int_0^t (t-\zeta)^{\upsilon-1}\zeta^{\varsigma-1}\mathrm{H}_4(\varsigma,I_h)d\zeta,\\
I(t)-I(0) &= \frac{\varsigma(1-\upsilon)t^{\varsigma-1}}{\mathscr{A}\mathscr{B}(\upsilon)}\mathrm{H}_5(t,I)+\frac{\upsilon\varsigma}{\mathscr{A}\mathscr{B}(\upsilon)\Gamma(\upsilon)}\int_0^t (t-\zeta)^{\upsilon-1}\zeta^{\varsigma-1}\mathrm{H}_5(\varsigma,I)d\zeta,\\
R(t)-R(0) &= \frac{\varsigma(1-\upsilon)t^{\varsigma-1}}{\mathscr{A}\mathscr{B}(\upsilon)}\mathrm{H}_6(t,R)+\frac{\upsilon\varsigma}{\mathscr{A}\mathscr{B}(\upsilon)\Gamma(\upsilon)}\int_0^t (t-\zeta)^{\upsilon-1}\zeta^{\varsigma-1}\mathrm{H}_6(\varsigma,R)d\zeta,\\
P(t)-P(0) &= \frac{\varsigma(1-\upsilon)t^{\varsigma-1}}{\mathscr{A}\mathscr{B}(\upsilon)}\mathrm{H}_7(t,P)+\frac{\upsilon\varsigma}{\mathscr{A}\mathscr{B}(\upsilon)\Gamma(\upsilon)}\int_0^t (t-\zeta)^{\upsilon-1}\zeta^{\varsigma-1}\mathrm{H}_7(\varsigma,P)d\zeta,
\end{aligned}
\tag{13}
$$

where

$$
\begin{cases}
\mathrm{H}_1(t,S)=A^{\upsilon}+m^{\upsilon}R-\frac{\alpha^{\upsilon}SP}{1+\omega_1^{\upsilon}P}-\frac{\beta^{\upsilon}S(I+I_h)}{1+\omega_2^{\upsilon}(I+I_h)}-\kappa^{\upsilon}S,\\
\mathrm{H}_2(t,Q)=\frac{\alpha^{\upsilon}SP}{1+\omega_1^{\upsilon}P}+\frac{\beta^{\upsilon}S(I+I_h)}{1+\omega_2^{\upsilon}(I+I_h)}-\gamma_1^{\upsilon}Q-\kappa^{\upsilon}Q,\\
\mathrm{H}_3(t,E)=\frac{(1-\sigma^{\upsilon})\alpha^{\upsilon}SP}{1+\omega_1^{\upsilon}P}+\frac{(1-\sigma^{\upsilon})\beta^{\upsilon}S(I+I_h)}{1+\omega_2^{\upsilon}(I+I_h)}-\theta^{\upsilon}\gamma_2^{\upsilon}E-(1-\sigma^{\upsilon})\theta^{\upsilon}\gamma_2^{\upsilon}E-\kappa^{\upsilon}E,\\
\mathrm{H}_4(t,I_h)=\gamma_1^{\upsilon}Q+(1-\theta^{\upsilon})\gamma_2^{\upsilon}E-\eta_1^{\upsilon}I_h-(\kappa^{\upsilon}+\delta^{\upsilon})I_h,\\
\mathrm{H}_5(t,I)=\theta^{\upsilon}\gamma_2^{\upsilon}E-\eta_2^{\upsilon}I-(\kappa^{\upsilon}+\delta^{\upsilon})I,\\
\mathrm{H}_6(t,R)=\eta_1^{\upsilon}I_h+\eta_2^{\upsilon}I-m^{\upsilon}R-\kappa^{\upsilon}R,\\
\mathrm{H}_7(t,P)=\mu^{\upsilon}I-\kappa_p^{\upsilon}P.
\end{cases}
$$

We make the following presumptions to prove our findings:

Â: The continuous functions $S(t), \hat{S}(t)$, $Q(t), \hat{Q}(t)$, $E(t), \hat{E}(t)$, $I_h(t), \hat{I}_h(t)$, $I(t), \hat{I}(t)$, $R(t), \hat{R}(t)$,
$P(t), \hat{P}(t) \in L[0, 1]$, such that $\|S\| \leq \varphi_1$, $\|I\| \leq \varphi_2$ for $\varphi_1, \varphi_2 > 0$.

Theorem 5.1 *If the presumption* Â *holds true and is satisfied* $\varphi_j < 1$ *for* $j \in N_1^7$, *then the kernels* $\mathrm{H}_1, \mathrm{H}_2, \mathrm{H}_3, \mathrm{H}_4, \mathrm{H}_5, \mathrm{H}_6, \mathrm{H}_7$,*are satisfying the Lipschitz condition and are contractions provided that* $\varphi_j < 1$ *for every* $j \in \mathrm{N}_1^7$.

Proof We start by demonstrating that the Lipschitz condition is fulfilled by $\mathrm{H}_1(t, S)$. When $S(t)$ and $\hat{S}(t)$ are used, we have

$$\begin{aligned}\left\|\mathrm{H}_1(t, S) - \mathrm{H}_1(t, \hat{S})\right\| &= \left\| \begin{array}{l} \left(A^\upsilon + m^\upsilon R - \frac{\alpha^\upsilon SP}{1+\omega_1^\upsilon P} - \frac{\beta^\upsilon S(I+I_h)}{1+\omega_2^\upsilon(I+I_h)} - \kappa^\upsilon S\right) \\ -\left(A^\upsilon + m^\upsilon R - \frac{\alpha^\upsilon \hat{S}P}{1+\omega_1^\upsilon P} - \frac{\beta^\upsilon \hat{S}(I+I_h)}{1+\omega_2^\upsilon(I+I_h)} - \kappa^\upsilon \hat{S}\right) \end{array} \right\| \\ &\leq \left[\frac{\alpha^\upsilon \|P\|}{1+\omega_1^\upsilon \|P\|} + \frac{\beta^\upsilon (I+I_h)}{1+\omega_2^\upsilon (I+I_h)} + \kappa^\upsilon\right] \left\|S - \hat{S}\right\| \\ &\leq \left[\frac{\alpha^\upsilon \mathrm{A}_1}{1+\omega_1^\upsilon \mathrm{A}_1} + \frac{\beta^\upsilon (\mathrm{A}_2+\mathrm{A}_3)}{1+\omega_2^\upsilon (\mathrm{A}_2+\mathrm{A}_3)} + \kappa^\upsilon\right] \left\|S - \hat{S}\right\| \\ &\leq \varphi_1 \left\|S - \hat{S}\right\|,\end{aligned}$$

where

$$\varphi_1 = \frac{\alpha^\upsilon \mathrm{A}_1}{1+\omega_1^\upsilon \mathrm{A}_1} + \frac{\beta^\upsilon (\mathrm{A}_2+\mathrm{A}_3)}{1+\omega_2^\upsilon (\mathrm{A}_2+\mathrm{A}_3)} + \kappa^\upsilon < 1.$$

Hence, it is true that H_1 meets the Lipschitz condition and $\varphi_1 < 1$. Next, we demonstrate that Lipschitz condition is satisfied by $\mathrm{H}_2(t, Q)$ for this $Q(t), \hat{Q}(t)$ we have

$$\begin{aligned}\left\|\mathrm{H}_2(t, Q) - \mathrm{H}_2(t, \hat{Q})\right\| &= \left\| \begin{array}{l} \left(\frac{\alpha^\upsilon SP}{1+\omega_1^\upsilon P} + \frac{\beta^\upsilon S(I+I_h)}{1+\omega_2^\upsilon(I+I_h)} - \gamma_1^\upsilon Q - \kappa^\upsilon Q\right) \\ -\left(\frac{\alpha^\upsilon SP}{1+\omega_1^\upsilon P} + \frac{\beta^\upsilon S(I+I_h)}{1+\omega_2^\upsilon(I+I_h)} - \gamma_1^\upsilon \hat{Q} - \kappa^\upsilon \hat{Q}\right) \end{array} \right\| \\ &\leq \left[\gamma_1^\upsilon + \kappa^\upsilon\right] \left\|Q - \hat{Q}\right\| \leq \varphi_2 \left\|Q - \hat{Q}\right\|,\end{aligned}$$

where $\varphi_2 = \gamma_1^\upsilon + \kappa^\upsilon < 1$.
Hence, it is true that H_2 satisfy the Lipschitz condition and $\varphi_2 < 1$. Next, we show that Lipschitz condition is fulfilled by $\mathrm{H}_3(t, E)$ for this $E(t), \hat{E}(t)$ we have

$$\begin{aligned}&\left\|\mathrm{H}_3(t, E) - \mathrm{H}_3(t, \hat{E})\right\| \\ &= \left\| \begin{array}{l} \left(\frac{(1-\sigma^\upsilon)\alpha^\upsilon SP}{1+\omega_1^\upsilon P} + \frac{(1-\sigma^\upsilon)\beta^\upsilon S(I+I_h)}{1+\omega_2^\upsilon(I+I_h)} - \theta^\upsilon \gamma_2^\upsilon E - (1-\sigma^\upsilon)\theta^\upsilon \gamma_2^\upsilon E - \kappa^\upsilon E\right) \\ -\left(\frac{(1-\sigma^\upsilon)\alpha^\upsilon SP}{1+\omega_1^\upsilon P} + \frac{(1-\sigma^\upsilon)\beta^\upsilon S(I+I_h)}{1+\omega_2^\upsilon(I+I_h)} - \theta^\upsilon \gamma_2 \hat{E} - (1-\sigma^\upsilon)\theta^\upsilon \gamma_2 \hat{E} - \kappa^\upsilon \hat{E}\right) \end{array} \right\| \\ &\leq \left[\theta^\upsilon \gamma_2^\upsilon + (1-\sigma^\upsilon)\theta^\upsilon \gamma_2^\upsilon + \kappa^\upsilon\right] \left\|E - \hat{E}\right\| \leq \varphi_3 \left\|E - \hat{E}\right\|,\end{aligned}$$

where $\varphi_3 = \theta^\upsilon \gamma_2^\upsilon + (1 - \sigma^\upsilon)\theta^\upsilon \gamma_2^\upsilon + \kappa^\upsilon < 1$.
Hence, it is true that H_3 fulfills the Lipschitz condition, and $\varphi_3 < 1$. Next, we demonstrate that Lipschitz condition is satisfied by $H_4(t, I_h)$ for this $I_h(t)$, $\hat{I}_h(t)$ we have

$$\begin{aligned}
\left\| H_4(t, I_h) - H_4(t, \hat{I}_h) \right\| &= \left\| \begin{array}{l} \left(\gamma_1^\upsilon Q + (1-\theta^\upsilon)\gamma_2^\upsilon E - \eta_1^\upsilon I_h - (\kappa^\upsilon + \delta^\upsilon) I_h\right) \\ - \left(\gamma_1^\upsilon Q + (1-\theta^\upsilon)\gamma_2^\upsilon E - \eta_1^\upsilon \hat{I}_h - (\kappa^\upsilon + \delta^\upsilon)\hat{I}_h\right) \end{array} \right\| \\
&\leq \left[\kappa^\upsilon + \delta^\upsilon\right] \left\| I_h - \hat{I}_h \right\| \\
&\leq \varphi_4 \left\| I_h - \hat{I}_h \right\|,
\end{aligned}$$

where $\varphi_4 = \eta_1^\upsilon + \kappa^\upsilon + \delta^\upsilon < 1$.
Hence, it is true that H_4 fulfills the Lipschitz condition, and $\varphi_4 < 1$. Next, we demonstrate that Lipschitz condition is satisfied by $H_5(t, I)$ for this $I(t)$, $\hat{I}(t)$ we have

$$\begin{aligned}
\left\| H_5(t, I) - H_5(t, \hat{I}) \right\| &= \left\| \begin{array}{l} \left(\theta^\upsilon \gamma_2^\upsilon E - \eta_2^\upsilon I - (\kappa^\upsilon + \delta^\upsilon) I\right) \\ - \left(\theta^\upsilon \gamma_2^\upsilon E - \eta_2^\upsilon \hat{I} - (\kappa^\upsilon + \delta^\upsilon)\hat{I}\right) \end{array} \right\| \\
&\leq \left[\eta_2^\upsilon + \kappa^\upsilon + \delta^\upsilon\right] \left\| I - \hat{I} \right\| \\
&\leq \varphi_5 \left\| I - \hat{I} \right\|,
\end{aligned}$$

where $\varphi_5 = \eta_2^\upsilon + \kappa^\upsilon + \delta^\upsilon < 1$.
Hence, it is true that H_5 fulfills the Lipschitz condition, and $\varphi_5 < 1$. Next, we demonstrate that Lipschitz condition is satisfied by $H_6(t, R)$ for this $R(t)$, $\hat{R}(t)$ we have

$$\begin{aligned}
\left\| H_6(t, R) - H_6(t, \hat{R}) \right\| &= \left\| \begin{array}{l} \left(\eta_1^\upsilon I_h + \eta_2^\upsilon I - m^\upsilon R - \kappa^\upsilon R\right) \\ - \left(\eta_1^\upsilon I_h + \eta_2^\upsilon I - m^\upsilon \hat{R} - \kappa^\upsilon \hat{R}\right) \end{array} \right\| \\
&\leq \left[m^\upsilon + \kappa^\upsilon\right] \left\| R - \hat{R} \right\| \\
&\leq \varphi_6 \left\| R - \hat{R} \right\|,
\end{aligned}$$

where $\varphi_6 = m^\upsilon + \kappa^\upsilon < 1$.
Hence, it is true that H_6 fulfills the Lipschitz condition, and $\varphi_6 < 1$. Next, we demonstrate that Lipschitz condition is satisfied by $H_7(t, P)$ for this $P(t)$, $\hat{P}(t)$ we have

$$\begin{aligned}
\left\| H_7(t, P) - H_7(t, \hat{P}) \right\| &= \left\| \left(\mu^\upsilon I - \kappa_p^\upsilon P\right) - \left(\mu^\upsilon I - \kappa_p^\upsilon \hat{P}\right) \right\| \\
&\leq \kappa_p^\upsilon \left\| P - \hat{P} \right\| \\
&\leq \varphi_7 \left\| P - \hat{P} \right\|,
\end{aligned}$$

where $\varphi_7 = \kappa_p^{\upsilon} < 1$.
Hence, it is true that H_7 fulfills the Lipschitz condition, and $\varphi_7 < 1$.
Finally, all of the functions satisfy the Lipschitz criteria, and the proof is completed. $\square$

We reformat the system as follows by using the kernels H_j, $j \in \mathrm{N}_1^7$, we have

$$\begin{cases} S(t) = \frac{\varsigma(1-\upsilon)t^{\varsigma-1}}{\mathscr{A}\mathscr{B}(\upsilon)}\mathrm{H}_1(t,S) + \frac{\upsilon\varsigma}{\mathscr{A}\mathscr{B}(\upsilon)\Gamma(\upsilon)}\int_0^t (t-\zeta)^{\upsilon-1}\zeta^{\varsigma-1}\mathrm{H}_2(\varsigma,S)d\zeta, \\ Q(t) = \frac{\varsigma(1-\upsilon)t^{\varsigma-1}}{\mathscr{A}\mathscr{B}(\upsilon)}\mathrm{H}_2(t,Q) + \frac{\upsilon\varsigma}{\mathscr{A}\mathscr{B}(\upsilon)\Gamma(\upsilon)}\int_0^t (t-\zeta)^{\upsilon-1}\zeta^{\varsigma-1}\mathrm{H}_2(\varsigma,Q)d\zeta, \\ E(t) = \frac{\varsigma(1-\upsilon)t^{\varsigma-1}}{\mathscr{A}\mathscr{B}(\upsilon)}\mathrm{H}_3(t,E) + \frac{\upsilon\varsigma}{\mathscr{A}\mathscr{B}(\upsilon)\Gamma(\upsilon)}\int_0^t (t-\zeta)^{\upsilon-1}\zeta^{\varsigma-1}\mathrm{H}_3(\varsigma,E)d\zeta, \\ I_h(t) = \frac{\varsigma(1-\upsilon)t^{\varsigma-1}}{\mathscr{A}\mathscr{B}(\upsilon)}\mathrm{H}_4(t,I_h) + \frac{\upsilon\varsigma}{\mathscr{A}\mathscr{B}(\upsilon)\Gamma(\upsilon)}\int_0^t (t-\zeta)^{\upsilon-1}\zeta^{\varsigma-1}\mathrm{H}_4(\varsigma,I_h)d\zeta, \\ I(t) = \frac{\varsigma(1-\upsilon)t^{\varsigma-1}}{\mathscr{A}\mathscr{B}(\upsilon)}\mathrm{H}_5(t,I) + \frac{\upsilon\varsigma}{\mathscr{A}\mathscr{B}(\upsilon)\Gamma(\upsilon)}\int_0^t (t-\zeta)^{\upsilon-1}\zeta^{\varsigma-1}\mathrm{H}_5(\varsigma,I)d\zeta, \\ R(t) = \frac{\varsigma(1-\upsilon)t^{\varsigma-1}}{\mathscr{A}\mathscr{B}(\upsilon)}\mathrm{H}_6(t,R) + \frac{\upsilon\varsigma}{\mathscr{A}\mathscr{B}(\upsilon)\Gamma(\upsilon)}\int_0^t (t-\zeta)^{\upsilon-1}\zeta^{\varsigma-1}\mathrm{H}_6(\varsigma,R)d\zeta, \\ P(t) = \frac{\varsigma(1-\upsilon)t^{\varsigma-1}}{\mathscr{A}\mathscr{B}(\upsilon)}\mathrm{H}_7(t,P) + \frac{\upsilon\varsigma}{\mathscr{A}\mathscr{B}(\upsilon)\Gamma(\upsilon)}\int_0^t (t-\zeta)^{\upsilon-1}\zeta^{\varsigma-1}\mathrm{H}_7(\varsigma,P)d\zeta. \end{cases}$$

We have,

$$\begin{cases} S_n(t) = \frac{\varsigma(1-\upsilon)t^{\varsigma-1}}{\mathscr{A}\mathscr{B}(\upsilon)}\mathrm{H}_1(t,S_{n-1}) + \frac{\upsilon\varsigma}{\mathscr{A}\mathscr{B}(\upsilon)\Gamma(\upsilon)}\int_0^t (t-\zeta)^{\upsilon-1}\zeta^{\varsigma-1}\mathrm{H}_2(\varsigma,S_{n-1})d\zeta, \\ Q_n(t) = \frac{\varsigma(1-\upsilon)t^{\varsigma-1}}{\mathscr{A}\mathscr{B}(\upsilon)}\mathrm{H}_2(t,Q_{n-1}) + \frac{\upsilon\varsigma}{\mathscr{A}\mathscr{B}(\upsilon)\Gamma(\upsilon)}\int_0^t (t-\zeta)^{\upsilon-1}\zeta^{\varsigma-1}\mathrm{H}_2(\varsigma,Q_{n-1})d\zeta, \\ E_{n-1}(t) = \frac{\varsigma(1-\upsilon)t^{\varsigma-1}}{\mathscr{A}\mathscr{B}(\upsilon)}\mathrm{H}_3(t,E_{n-1}) + \frac{\upsilon\varsigma}{\mathscr{A}\mathscr{B}(\upsilon)\Gamma(\upsilon)}\int_0^t (t-\zeta)^{\upsilon-1}\zeta^{\varsigma-1}\mathrm{H}_3(\varsigma,E_{n-1})d\zeta, \\ I_{hn}(t) = \frac{\varsigma(1-\upsilon)t^{\varsigma-1}}{\mathscr{A}\mathscr{B}(\upsilon)}\mathrm{H}_4(t,I_{hn-1}) + \frac{\upsilon\varsigma}{\mathscr{A}\mathscr{B}(\upsilon)\Gamma(\upsilon)}\int_0^t (t-\zeta)^{\upsilon-1}\zeta^{\varsigma-1}\mathrm{H}_4(\varsigma,I_{hn-1})d\zeta, \\ I_n(t) = \frac{\varsigma(1-\upsilon)t^{\varsigma-1}}{\mathscr{A}\mathscr{B}(\upsilon)}\mathrm{H}_5(t,I_{n-1}) + \frac{\upsilon\varsigma}{\mathscr{A}\mathscr{B}(\upsilon)\Gamma(\upsilon)}\int_0^t (t-\zeta)^{\upsilon-1}\zeta^{\varsigma-1}\mathrm{H}_5(\varsigma,I_{n-1})d\zeta, \\ R_n(t) = \frac{\varsigma(1-\upsilon)t^{\varsigma-1}}{\mathscr{A}\mathscr{B}(\upsilon)}\mathrm{H}_6(t,R_{n-1}) + \frac{\upsilon\varsigma}{\mathscr{A}\mathscr{B}(\upsilon)\Gamma(\upsilon)}\int_0^t (t-\zeta)^{\upsilon-1}\zeta^{\varsigma-1}\mathrm{H}_6(\varsigma,R_{n-1})d\zeta, \\ P_n(t) = \frac{\varsigma(1-\upsilon)t^{\varsigma-1}}{\mathscr{A}\mathscr{B}(\upsilon)}\mathrm{H}_7(t,P_{n-1}) + \frac{\upsilon\varsigma}{\mathscr{A}\mathscr{B}(\upsilon)\Gamma(\upsilon)}\int_0^t (t-\zeta)^{\upsilon-1}\zeta^{\varsigma-1}\mathrm{H}_7(\varsigma,P_{n-1})d\zeta. \end{cases}$$

Next, we consider the differences as follows:

$$\begin{aligned} \Delta S_{n+1}(t) &= S_{n+1} - S_n = \frac{\varsigma(1-\upsilon)t^{\varsigma-1}}{\mathscr{A}\mathscr{B}(\upsilon)}\left(\mathrm{H}_1(t,S_n) - \mathrm{H}_1(t,S_{n-1})\right) \\ &\quad + \frac{\upsilon\varsigma}{\mathscr{A}\mathscr{B}(\upsilon)\Gamma(\upsilon)}\int_0^t (t-\zeta)^{\upsilon-1}\zeta^{\varsigma-1}\left(\mathrm{H}_1(t,S_n) - \mathrm{H}_1(t,S_{n-1})\right)d\zeta, \\ \Delta Q_{n+1}(t) &= Q_{n+1} - Q_n \\ &= \frac{\varsigma(1-\upsilon)t^{\varsigma-1}}{\mathscr{A}\mathscr{B}(\upsilon)}\left(\mathrm{H}_2(t,Q_n) - \mathrm{H}_2(t,Q_{n-1})\right) \\ &\quad + \frac{\upsilon\varsigma}{\mathscr{A}\mathscr{B}(\upsilon)\Gamma(\upsilon)}\int_0^t (t-\zeta)^{\upsilon-1}\zeta^{\varsigma-1}\left(\mathrm{H}_2(t,Q_n) - \mathrm{H}_2(t,Q_{n-1})\right)d\zeta, \\ \Delta E_{n+1}(t) &= E_{n+1} - E_n \\ &= \frac{\varsigma(1-\upsilon)t^{\varsigma-1}}{\mathscr{A}\mathscr{B}(\upsilon)}\left(\mathrm{H}_3(t,E_n) - \mathrm{H}_3(t,E_{n-1})\right) \end{aligned}$$

$$
\begin{aligned}
&+\frac{\upsilon\varsigma}{\mathscr{A}\mathscr{B}(\upsilon)\Gamma(\upsilon)}\int_0^t (t-\zeta)^{\upsilon-1}\zeta^{\varsigma-1}\left(\mathrm{H}_3(t,E_n)-\mathrm{H}_3(t,E_{n-1})\right)d\zeta,\\
\Delta I_{hn+1}(t) &= I_{hn+1}-I_{hn}\\
&=\frac{\varsigma(1-\upsilon)t^{\varsigma-1}}{\mathscr{A}\mathscr{B}(\upsilon)}\left(\mathrm{H}_4(t,I_{hn})-\mathrm{H}_4(t,I_{hn-1})\right)\\
&+\frac{\upsilon\varsigma}{\mathscr{A}\mathscr{B}(\upsilon)\Gamma(\upsilon)}\int_0^t (t-\zeta)^{\upsilon-1}\zeta^{\varsigma-1}\left(\mathrm{H}_4(t,I_{hn})-\mathrm{H}_4(t,I_{hn-1})\right)d\zeta,\\
\Delta I_{n+1}(t) &= I_{n+1}-I_n\\
&=\frac{\varsigma(1-\upsilon)t^{\varsigma-1}}{\mathscr{A}\mathscr{B}(\upsilon)}\left(\mathrm{H}_5(t,I_n)-\mathrm{H}_5(t,I_{n-1})\right)\\
&+\frac{\upsilon\varsigma}{\mathscr{A}\mathscr{B}(\upsilon)\Gamma(\upsilon)}\int_0^t (t-\zeta)^{\upsilon-1}\zeta^{\varsigma-1}\left(\mathrm{H}_5(t,I_n)-\mathrm{H}_5(t,I_{n-1})\right)d\zeta,\\
\Delta R_{n+1}(t) &= R_{n+1}-R_n\\
&=\frac{\varsigma(1-\upsilon)t^{\varsigma-1}}{\mathscr{A}\mathscr{B}(\upsilon)}\left(\mathrm{H}_6(t,R_n)-\mathrm{H}_6(t,R_{n-1})\right)\\
&+\frac{\upsilon\varsigma}{\mathscr{A}\mathscr{B}(\upsilon)\Gamma(\upsilon)}\int_0^t (t-\zeta)^{\upsilon-1}\zeta^{\varsigma-1}\left(\mathrm{H}_6(t,R_n)-\mathrm{H}_6(t,R_{n-1})\right)d\zeta,\\
\Delta P_{n+1}(t) &= P_{n+1}-P_n\\
&=\frac{\varsigma(1-\upsilon)t^{\varsigma-1}}{\mathscr{A}\mathscr{B}(\upsilon)}\left(\mathrm{H}_7(t,P_n)-\mathrm{H}_7(t,P_{n-1})\right)\\
&+\frac{\upsilon\varsigma}{\mathscr{A}\mathscr{B}(\upsilon)\Gamma(\upsilon)}\int_0^t (t-\zeta)^{\upsilon-1}\zeta^{\varsigma-1}\left(\mathrm{H}_7(t,P_n)-\mathrm{H}_7(t,P_{n-1})\right)d\zeta.
\end{aligned}
$$

Taking the aforementioned system's norms for both sides,

$$
\begin{aligned}
\|\Delta S_{n+1}(t)\| &\le \frac{\varsigma(1-\upsilon)t^{\varsigma-1}}{\mathscr{A}\mathscr{B}(\upsilon)}\left\|\left(\mathrm{H}_1(t,S_n)-\mathrm{H}_1(t,S_{n-1})\right)\right\|\\
&+\frac{\upsilon\varsigma}{\mathscr{A}\mathscr{B}(\upsilon)\Gamma(\upsilon)}\int_0^t (t-\zeta)^{\upsilon-1}\zeta^{\varsigma-1}\left\|\left(\mathrm{H}_1(t,S_n)-\mathrm{H}_1(t,S_{n-1})\right)\right\|d\zeta,\\
\|\Delta Q_{n+1}(t)\| &\le \frac{\varsigma(1-\upsilon)t^{\varsigma-1}}{\mathscr{A}\mathscr{B}(\upsilon)}\left\|\left(\mathrm{H}_2(t,Q_n)-\mathrm{H}_2(t,Q_{n-1})\right)\right\|\\
&+\frac{\upsilon\varsigma}{\mathscr{A}\mathscr{B}(\upsilon)\Gamma(\upsilon)}\int_0^t (t-\zeta)^{\upsilon-1}\zeta^{\varsigma-1}\left\|\left(\mathrm{H}_2(t,Q_n)-\mathrm{H}_2(t,Q_{n-1})\right)\right\|d\zeta,\\
\|\Delta E_{n+1}(t)\| &\le \frac{\varsigma(1-\upsilon)t^{\varsigma-1}}{\mathscr{A}\mathscr{B}(\upsilon)}\left\|\left(\mathrm{H}_3(t,E_n)-\mathrm{H}_3(t,E_{n-1})\right)\right\|\\
&+\frac{\upsilon\varsigma}{\mathscr{A}\mathscr{B}(\upsilon)\Gamma(\upsilon)}\int_0^t (t-\zeta)^{\upsilon-1}\zeta^{\varsigma-1}\left\|\left(\mathrm{H}_3(t,E_n)-\mathrm{H}_3(t,E_{n-1})\right)\right\|d\zeta,\\
\|\Delta I_{hn+1}(t)\| &\le \frac{\varsigma(1-\upsilon)t^{\varsigma-1}}{\mathscr{A}\mathscr{B}(\upsilon)}\left\|\left(\mathrm{H}_4(t,I_{hn})-\mathrm{H}_4(t,I_{hn-1})\right)\right\|
\end{aligned}
$$

$$
\begin{aligned}
&+\frac{\upsilon\varsigma}{\mathscr{A}\mathscr{B}(\upsilon)\Gamma(\upsilon)}\int_0^t (t-\zeta)^{\upsilon-1}\zeta^{\varsigma-1}\left\|(\mathrm{H}_4(t,I_{hn})-\mathrm{H}_4(t,I_{hn-1}))\right\| d\zeta,\\
\|\Delta I_{n+1}(t)\| \leq{}& \frac{\varsigma(1-\upsilon)t^{\varsigma-1}}{\mathscr{A}\mathscr{B}(\upsilon)}\left\|(\mathrm{H}_5(t,I_n)-\mathrm{H}_5(t,I_{n-1}))\right\|\\
&+\frac{\upsilon\varsigma}{\mathscr{A}\mathscr{B}(\upsilon)\Gamma(\upsilon)}\int_0^t (t-\zeta)^{\upsilon-1}\zeta^{\varsigma-1}\left\|(\mathrm{H}_5(t,I_n)-\mathrm{H}_5(t,I_{n-1}))\right\| d\zeta,\\
\|\Delta R_{n+1}(t)\| \leq{}& \frac{\varsigma(1-\upsilon)t^{\varsigma-1}}{\mathscr{A}\mathscr{B}(\upsilon)}\left\|(\mathrm{H}_6(t,R_n)-\mathrm{H}_6(t,R_{n-1}))\right\|\\
&+\frac{\upsilon\varsigma}{\mathscr{A}\mathscr{B}(\upsilon)\Gamma(\upsilon)}\int_0^t (t-\zeta)^{\upsilon-1}\zeta^{\varsigma-1}\left\|(\mathrm{H}_6(t,R_n)-\mathrm{H}_6(t,R_{n-1}))\right\| d\zeta,\\
\|\Delta P_{n+1}(t)\| \leq{}& \frac{\varsigma(1-\upsilon)t^{\varsigma-1}}{\mathscr{A}\mathscr{B}(\upsilon)}\left\|(\mathrm{H}_7(t,P_n)-\mathrm{H}_7(t,P_{n-1}))\right\|\\
&+\frac{\upsilon\varsigma}{\mathscr{A}\mathscr{B}(\upsilon)\Gamma(\upsilon)}\int_0^t (t-\zeta)^{\upsilon-1}\zeta^{\varsigma-1}\left\|(\mathrm{H}_7(t,P_n)-\mathrm{H}_7(t,P_{n-1}))\right\| d\zeta.
\end{aligned}
$$

Theorem 5.2 *If the following is true, then there is a solution to the fractal fractional-order COVID-19 model (8).*

$$
\Omega=\max\left[\varphi_1,\varphi_2,\varphi_3,\varphi_4,\varphi_5,\varphi_6,\varphi_7\right]<1.
$$

Proof We define the function

$$
\begin{aligned}
\mathrm{Z1}_n(t)&=S_{n+1}(t)-S(t),\\
\mathrm{Z2}_n(t)&=Q_{n+1}(t)-Q(t),\\
\mathrm{Z3}_n(t)&=E_{n+1}(t)-E(t),\\
\mathrm{Z4}_n(t)&=I_{hn+1}(t)-I_h(t),\\
\mathrm{Z5}_n(t)&=I_{n+1}(t)-I(t),\\
\mathrm{Z6}_n(t)&=R_{n+1}(t)-R(t),\\
\mathrm{Z7}_n(t)&=P_{n+1}(t)-P(t).
\end{aligned}
$$

Taking the aforementioned system's norms we have,

$$
\begin{aligned}
\|\mathrm{Z1}_n(t)\| &= \|S_{n+1}(t)-S(t)\|\\
&=\frac{\varsigma(1-\upsilon)t^{\varsigma-1}}{\mathscr{A}\mathscr{B}(\upsilon)}\left\|(\mathrm{H}_1(t,S_n)-\mathrm{H}_1(t,S))\right\|\\
&\quad+\frac{\upsilon\varsigma}{\mathscr{A}\mathscr{B}(\upsilon)\Gamma(\upsilon)}\int_0^t (t-\zeta)^{\upsilon-1}\zeta^{\varsigma-1}\left\|(\mathrm{H}_1(t,S_n)-\mathrm{H}_1(t,S))\right\| d\zeta\\
&\leq \frac{\upsilon\varsigma}{\mathscr{A}\mathscr{B}(\upsilon)\Gamma(\upsilon)}\int_0^t (t-\zeta)^{\upsilon-1}\zeta^{\varsigma-1}\varphi_1\|S_n-S\|\, d\zeta\\
&\quad+\frac{\varsigma(1-\upsilon)t^{\varsigma-1}}{\mathscr{A}\mathscr{B}(\upsilon)}\varphi_1\|S_n-S\|\\
&\leq\left[\frac{\upsilon\varsigma\Gamma(\varsigma)}{\mathscr{A}\mathscr{B}(\upsilon)\Gamma(\upsilon+\varsigma)}+\frac{\varsigma(1-\upsilon)}{\mathscr{A}\mathscr{B}(\upsilon)}\right]\varphi_1\|S_n-S\|
\end{aligned}
$$

$$\leq \left[\frac{\upsilon\varsigma\Gamma(\varsigma)}{\mathscr{A}\mathscr{B}(\upsilon)\Gamma(\upsilon+\varsigma)} + \frac{\varsigma(1-\upsilon)}{\mathscr{A}\mathscr{B}(\upsilon)} \right]^n \lambda^n \left\| S_n - S \right\|,$$

where $\lambda < 1$ and $n \to \infty$, $S_n \to S$ similarly we have

$$\begin{aligned}
\|Z2_n\| &\leq \left[\tfrac{\upsilon\varsigma\Gamma(\varsigma)}{\mathscr{A}\mathscr{B}(\upsilon)\Gamma(\upsilon+\varsigma)} + \tfrac{\varsigma(1-\upsilon)}{\mathscr{A}\mathscr{B}(\upsilon)} \right]^n \lambda^n \left\| Q_n - Q \right\|, \\
\|Z3_n\| &\leq \left[\tfrac{\upsilon\varsigma\Gamma(\varsigma)}{\mathscr{A}\mathscr{B}(\upsilon)\Gamma(\upsilon+\varsigma)} + \tfrac{\varsigma(1-\upsilon)}{\mathscr{A}\mathscr{B}(\upsilon)} \right]^n \lambda^n \left\| E_n - E \right\|, \\
\|Z4_n\| &\leq \left[\tfrac{\upsilon\varsigma\Gamma(\varsigma)}{\mathscr{A}\mathscr{B}(\upsilon)\Gamma(\upsilon+\varsigma)} + \tfrac{\varsigma(1-\upsilon)}{\mathscr{A}\mathscr{B}(\upsilon)} \right]^n \lambda^n \left\| I_{hn} - I_n \right\|, \\
\|Z5_n\| &\leq \left[\tfrac{\upsilon\varsigma\Gamma(\varsigma)}{\mathscr{A}\mathscr{B}(\upsilon)\Gamma(\upsilon+\varsigma)} + \tfrac{\varsigma(1-\upsilon)}{\mathscr{A}\mathscr{B}(\upsilon)} \right]^n \lambda^n \left\| I_n - I \right\|, \\
\|Z6_n\| &\leq \left[\tfrac{\upsilon\varsigma\Gamma(\varsigma)}{\mathscr{A}\mathscr{B}(\upsilon)\Gamma(\upsilon+\varsigma)} + \tfrac{\varsigma(1-\upsilon)}{\mathscr{A}\mathscr{B}(\upsilon)} \right]^n \lambda^n \left\| R_n - R \right\|, \\
\|Z7_n\| &\leq \left[\tfrac{\upsilon\varsigma\Gamma(\varsigma)}{\mathscr{A}\mathscr{B}(\upsilon)\Gamma(\upsilon+\varsigma)} + \tfrac{\varsigma(1-\upsilon)}{\mathscr{A}\mathscr{B}(\upsilon)} \right]^n \lambda^n \left\| P_n - P \right\|.
\end{aligned}$$

As a result, we observe that $Zj_n(t) \to 0$ as $n \to \infty$ for $j \in N_1^7$ and $\lambda < 1$ which complete the proof. □

Theorem 5.3 *If the following is true, then the fractal-fractional model (8) has a unique solution:*

$$\left[\frac{\upsilon\varsigma\Gamma(\varsigma)}{\mathscr{A}\mathscr{B}(\upsilon)\Gamma(\upsilon+\varsigma)} + \frac{\varsigma(1-\upsilon)}{\mathscr{A}\mathscr{B}(\upsilon)} \right] \Im_j \leq 1,\ j \in N_1^7.$$

Proof Let's take into account the contradiction that the model's fractal-fractional solution can have more than one solution. $\tilde{S}(t)$, $\tilde{Q}(t)$, $\tilde{E}(t)$,$\tilde{I}_h(t)$,$\tilde{I}(t)$,$\tilde{R}(t)$,$\tilde{P}(t)$ such that

$$\begin{cases}
\tilde{S}(t) = \frac{\varsigma(1-\upsilon)t^{\varsigma-1}}{\mathscr{A}\mathscr{B}(\upsilon)}\mathrm{H}_1(t,\tilde{S}) + \frac{\upsilon\varsigma}{\mathscr{A}\mathscr{B}(\upsilon)\Gamma(\upsilon)}\int_0^t (t-\zeta)^{\upsilon-1}\zeta^{\varsigma-1}\mathrm{H}_1(\zeta,\tilde{S})d\zeta, \\
\tilde{Q}(t) = \frac{\varsigma(1-\upsilon)t^{\varsigma-1}}{\mathscr{A}\mathscr{B}(\upsilon)}\mathrm{H}_2(t,\tilde{Q}) + \frac{\upsilon\varsigma}{\mathscr{A}\mathscr{B}(\upsilon)\Gamma(\upsilon)}\int_0^t (t-\zeta)^{\upsilon-1}\zeta^{\varsigma-1}\mathrm{H}_2(\zeta,\tilde{Q})d\zeta, \\
\tilde{E}(t) = \frac{\varsigma(1-\upsilon)t^{\varsigma-1}}{\mathscr{A}\mathscr{B}(\upsilon)}\mathrm{H}_3(t,\tilde{E}) + \frac{\upsilon\varsigma}{\mathscr{A}\mathscr{B}(\upsilon)\Gamma(\upsilon)}\int_0^t (t-\zeta)^{\upsilon-1}\zeta^{\varsigma-1}\mathrm{H}_3(\zeta,\tilde{E})d\zeta, \\
\tilde{I}_h(t) = \frac{\varsigma(1-\upsilon)t^{\varsigma-1}}{\mathscr{A}\mathscr{B}(\upsilon)}\mathrm{H}_4(t,\tilde{I}_h) + \frac{\upsilon\varsigma}{\mathscr{A}\mathscr{B}(\upsilon)\Gamma(\upsilon)}\int_0^t (t-\zeta)^{\upsilon-1}\zeta^{\varsigma-1}\mathrm{H}_4(\zeta,\tilde{I}_h)d\zeta, \\
\tilde{I}(t) = \frac{\varsigma(1-\upsilon)t^{\varsigma-1}}{\mathscr{A}\mathscr{B}(\upsilon)}\mathrm{H}_5(t,\tilde{I}) + \frac{\upsilon\varsigma}{\mathscr{A}\mathscr{B}(\upsilon)\Gamma(\upsilon)}\int_0^t (t-\zeta)^{\upsilon-1}\zeta^{\varsigma-1}\mathrm{H}_5(\zeta,\tilde{I})d\zeta, \\
\tilde{R}(t) = \frac{\varsigma(1-\upsilon)t^{\varsigma-1}}{\mathscr{A}\mathscr{B}(\upsilon)}\mathrm{H}_6(t,\tilde{R}) + \frac{\upsilon\varsigma}{\mathscr{A}\mathscr{B}(\upsilon)\Gamma(\upsilon)}\int_0^t (t-\zeta)^{\upsilon-1}\zeta^{\varsigma-1}\mathrm{H}_6(\zeta,\tilde{R})d\zeta, \\
\tilde{P}(t) = \frac{\varsigma(1-\upsilon)t^{\varsigma-1}}{\mathscr{A}\mathscr{B}(\upsilon)}\mathrm{H}_7(t,\tilde{P}) + \frac{\upsilon\varsigma}{\mathscr{A}\mathscr{B}(\upsilon)\Gamma(\upsilon)}\int_0^t (t-\zeta)^{\upsilon-1}\zeta^{\varsigma-1}\mathrm{H}_7(\zeta,\tilde{P})d\zeta.
\end{cases}$$

Now taking differences of $S(t)$, $\tilde{S}(t)$ and then take norm, we have

$$\begin{aligned}
\left\| S(t) - \tilde{S}(t) \right\| &= \frac{\upsilon\varsigma}{\mathscr{A}\mathscr{B}(\upsilon)\Gamma(\upsilon)} \int_0^t (t-\zeta)^{\upsilon-1}\zeta^{\varsigma-1} \left\| \mathrm{H}_1(\zeta,S) - \mathrm{H}_1(\zeta,\tilde{S}) \right\| d\zeta \\
&\quad + \frac{\varsigma(1-\upsilon)t^{\varsigma-1}}{\mathscr{A}\mathscr{B}(\upsilon)} \left\| \mathrm{H}_1(t,S) - \mathrm{H}_1(t,\tilde{S}) \right\|
\end{aligned}$$

$$
\begin{aligned}
&\leq \frac{\upsilon\varsigma}{\mathscr{A}\mathscr{B}(\upsilon)\Gamma(\upsilon)} \int_0^t (t-\zeta)^{\upsilon-1}\zeta^{\varsigma-1}\Theta_1 \left\| S-\tilde{S} \right\| d\zeta + \frac{\varsigma(1-\upsilon)t^{\varsigma-1}}{\mathscr{A}\mathscr{B}(\upsilon)}\Theta_1 \left\| S-\tilde{S} \right\| \\
&\leq \left[\frac{\upsilon\varsigma\Gamma(\varsigma)}{\mathscr{A}\mathscr{B}(\upsilon)\Gamma(\upsilon+\varsigma)} + \frac{\varsigma(1-\upsilon)}{\mathscr{A}\mathscr{B}(\upsilon)} \right] \Theta_1 \left\| S-\tilde{S} \right\| \\
&\left\| S-\tilde{S} \right\| - \left[\frac{\upsilon\varsigma\Gamma(\varsigma)}{\mathscr{A}\mathscr{B}(\upsilon)\Gamma(\upsilon+\varsigma)} + \frac{\varsigma(1-\upsilon)}{\mathscr{A}\mathscr{B}(\upsilon)} \right] \Theta_1 \left\| S-\tilde{S} \right\| \leq 0 \\
&\left[1 - \left(\frac{\upsilon\varsigma\Gamma(\varsigma)}{\mathscr{A}\mathscr{B}(\upsilon)\Gamma(\upsilon+\varsigma)} + \frac{\varsigma(1-\upsilon)}{\mathscr{A}\mathscr{B}(\upsilon)} \right) \Theta_1 \right] \left\| S-\tilde{S} \right\| \leq 0.
\end{aligned}
$$

The inequality mentioned above is accurate if

$$
\begin{aligned}
&\left\| S-\tilde{S} \right\| = 0, \\
&\Rightarrow S = \tilde{S}. \\
&\left\| Q-\tilde{Q} \right\| \leq \left[\frac{\upsilon\varsigma\Gamma(\varsigma)}{\mathscr{A}\mathscr{B}(\upsilon)\Gamma(\upsilon+\varsigma)} + \frac{\varsigma(1-\upsilon)}{\mathscr{A}\mathscr{B}(\upsilon)} \right] \Theta_2 \left\| Q-\tilde{Q} \right\| \\
&\left[1 - \left(\frac{\upsilon\varsigma\Gamma(\varsigma)}{\mathscr{A}\mathscr{B}(\upsilon)\Gamma(\upsilon+\varsigma)} + \frac{\varsigma(1-\upsilon)}{\mathscr{A}\mathscr{B}(\upsilon)} \right) \Theta_2 \right] \left\| Q-\tilde{Q} \right\| \leq 0.
\end{aligned}
$$

The inequality mentioned above is accurate if

$$
\begin{aligned}
&\left\| Q-\tilde{Q} \right\| = 0, \\
&\Rightarrow Q = \tilde{Q}. \\
&\left\| E-\tilde{E} \right\| \leq \left[\frac{\upsilon\varsigma\Gamma(\varsigma)}{\mathscr{A}\mathscr{B}(\upsilon)\Gamma(\upsilon+\varsigma)} + \frac{\varsigma(1-\upsilon)}{\mathscr{A}\mathscr{B}(\upsilon)} \right] \Theta_3 \left\| E-\tilde{E} \right\| \\
&\left[1 - \left(\frac{\upsilon\varsigma\Gamma(\varsigma)}{\mathscr{A}\mathscr{B}(\upsilon)\Gamma(\upsilon+\varsigma)} + \frac{\varsigma(1-\upsilon)}{\mathscr{A}\mathscr{B}(\upsilon)} \right) \Theta_3 \right] \left\| E-\tilde{E} \right\| \leq 0.
\end{aligned}
$$

The inequality mentioned above is accurate if

$$
\begin{aligned}
&\left\| E-\tilde{E} \right\| = 0, \\
&\Rightarrow E = \tilde{E}. \\
&\left\| I_h-\tilde{I}_h \right\| \leq \left[\frac{\upsilon\varsigma\Gamma(\varsigma)}{\mathscr{A}\mathscr{B}(\upsilon)\Gamma(\upsilon+\varsigma)} + \frac{\varsigma(1-\upsilon)}{AB(\upsilon)} \right] \Theta_4 \left\| I_h-\tilde{I}_h \right\| \\
&\left[1 - \left(\frac{\upsilon\varsigma\Gamma(\varsigma)}{\mathscr{A}\mathscr{B}(\upsilon)\Gamma(\upsilon+\varsigma)} + \frac{\varsigma(1-\upsilon)}{\mathscr{A}\mathscr{B}(\upsilon)} \right) \Theta_4 \right] \left\| I_h-\tilde{I}_h \right\| \leq 0.
\end{aligned}
$$

The inequality mentioned above is accurate if

$$
\begin{aligned}
&\left\| I_h-\tilde{I}_h \right\| = 0, \\
&\Rightarrow I_h = \tilde{I}_h.
\end{aligned}
$$

$$\left\|I-\tilde{I}\right\| \leq \left[\frac{\upsilon\varsigma\Gamma(\varsigma)}{\mathscr{A}\mathscr{B}(\upsilon)\Gamma(\upsilon+\varsigma)}+\frac{\varsigma(1-\upsilon)}{\mathscr{A}\mathscr{B}(\upsilon)}\right]\Theta_5\left\|I-\tilde{I}\right\|$$
$$\left[1-\left(\frac{\upsilon\varsigma\Gamma(\varsigma)}{\mathscr{A}\mathscr{B}(\upsilon)\Gamma(\upsilon+\varsigma)}+\frac{\varsigma(1-\upsilon)}{\mathscr{A}\mathscr{B}(\upsilon)}\right)\Theta_5\right]\left\|I-\tilde{I}\right\| \leq 0.$$

The inequality mentioned above is accurate if

$$\left\|I-\tilde{I}\right\| = 0,$$
$$\Rightarrow I=\tilde{I}.$$
$$\left\|R-\tilde{R}\right\| \leq \left[\frac{\upsilon\varsigma\Gamma(\varsigma)}{\mathscr{A}\mathscr{B}(\upsilon)\Gamma(\upsilon+\varsigma)}+\frac{\varsigma(1-\upsilon)}{\mathscr{A}\mathscr{B}(\upsilon)}\right]\Theta_6\left\|R-\tilde{R}\right\|$$
$$\left[1-\left(\frac{\upsilon\varsigma\Gamma(\varsigma)}{\mathscr{A}\mathscr{B}(\upsilon)\Gamma(\upsilon+\varsigma)}+\frac{\varsigma(1-\upsilon)}{\mathscr{A}\mathscr{B}(\upsilon)}\right)\Theta_6\right]\left\|R-\tilde{R}\right\| \leq 0.$$

The inequality mentioned above is accurate if

$$\left\|R-\tilde{R}\right\| = 0,$$
$$\Rightarrow R=\tilde{R}.$$

Similarly

$$\left\|P-\tilde{P}\right\| \leq \left[\frac{\upsilon\varsigma\Gamma(\varsigma)}{\mathscr{A}\mathscr{B}(\upsilon)\Gamma(\upsilon+\varsigma)}+\frac{\varsigma(1-\upsilon)}{\mathscr{A}\mathscr{B}(\upsilon)}\right]\Theta_7\left\|P-\tilde{P}\right\|$$
$$\left[1-\left(\frac{\upsilon\varsigma\Gamma(\varsigma)}{\mathscr{A}\mathscr{B}(\upsilon)\Gamma(\upsilon+\varsigma)}+\frac{\varsigma(1-\upsilon)}{\mathscr{A}\mathscr{B}(\upsilon)}\right)\Theta_7\right]\left\|P-\tilde{P}\right\| \leq 0.$$

The inequality mentioned above is accurate if

$$\left\|P-\tilde{P}\right\| = 0,$$
$$\Rightarrow P=\tilde{P}.$$

Therefore, (8) has a unique solution. □

6 Hyers-Ulams stability

Definition 6.1 Proposed system (8) is regarded be Hyers-Ulam stable if a constant $\ell_j > 0,\ j \in N_1^7$ satisfying for every $\wp_j > 0,\ j \in N_1^7$.

$$\begin{cases} \left| S(t) - \frac{\varsigma(1-\upsilon)t^{\varsigma-1}}{\mathscr{AB}(\upsilon)} \mathrm{H}_1(t,S) - \frac{\upsilon\varsigma}{\mathscr{AB}(\upsilon)\Gamma(\upsilon)} \int_0^t (t-\zeta)^{\upsilon-1}\zeta^{\varsigma-1} \mathrm{H}_1(\zeta, S(\zeta))d\zeta \right| \leq \wp_1, \\ \left| Q(t) - \frac{\varsigma(1-\upsilon)t^{\varsigma-1}}{\mathscr{AB}(\upsilon)} \mathrm{H}_2(t,Q) - \frac{\upsilon\varsigma}{\mathscr{AB}(\upsilon)\Gamma(\upsilon)} \int_0^t (t-\zeta)^{\upsilon-1}\zeta^{\varsigma-1} \mathrm{H}_2(\zeta, Q(\zeta))d\zeta \right| \leq \wp_2, \\ \left| E(t) - \frac{\varsigma(1-\upsilon)t^{\varsigma-1}}{\mathscr{AB}(\upsilon)} \mathrm{H}_3(t,E) - \frac{\upsilon\varsigma}{\mathscr{AB}(\upsilon)\Gamma(\upsilon)} \int_0^t (t-\zeta)^{\upsilon-1}\zeta^{\varsigma-1} \mathrm{H}_3(\zeta, E(\zeta))d\zeta \right| \leq \wp_3, \\ \left| I_h(t) - \frac{\varsigma(1-\upsilon)t^{\varsigma-1}}{\mathscr{AB}(\upsilon)} \mathrm{H}_4(t,I_h) - \frac{\upsilon\varsigma}{\mathscr{AB}(\upsilon)\Gamma(\upsilon)} \int_0^t (t-\zeta)^{\upsilon-1}\zeta^{\varsigma-1} \mathrm{H}_4(\zeta, I_h(\zeta))d\zeta \right| \leq \wp_4, \\ \left| I(t) - \frac{\varsigma(1-\upsilon)t^{\varsigma-1}}{\mathscr{AB}(\upsilon)} \mathrm{H}_5(t,I) - \frac{\upsilon\varsigma}{\mathscr{AB}(\upsilon)\Gamma(\upsilon)} \int_0^t (t-\zeta)^{\upsilon-1}\zeta^{\varsigma-1} \mathrm{H}_5(\zeta, I(\zeta))d\zeta \right| \leq \wp_5, \\ \left| R(t) - \frac{\varsigma(1-\upsilon)t^{\varsigma-1}}{\mathscr{AB}(\upsilon)} \mathrm{H}_6(t,R) - \frac{\upsilon\varsigma}{\mathscr{AB}(\upsilon)\Gamma(\upsilon)} \int_0^t (t-\zeta)^{\upsilon-1}\zeta^{\varsigma-1} \mathrm{H}_6(\zeta, R(\zeta))d\zeta \right| \leq \wp_6, \\ \left| P(t) - \frac{\varsigma(1-\upsilon)t^{\varsigma-1}}{\mathscr{AB}(\upsilon)} \mathrm{H}_7(t,P) - \frac{\upsilon\varsigma}{\mathscr{AB}(\upsilon)\Gamma(\upsilon)} \int_0^t (t-\zeta)^{\upsilon-1}\zeta^{\varsigma-1} \mathrm{H}_7(\zeta, P(\zeta))d\zeta \right| \leq \wp_7. \end{cases}$$

There is an approximation to the model (1), $S^\bullet(t)$, $Q^\bullet(t)$, $E^\bullet(t)$, $I_h^\bullet$,$R^\bullet(t)$, $P^\bullet(t)$ that fulfills the provided model, such that

$$\begin{aligned} \left\| S(t) - S^\bullet(t) \right\| &= \frac{\upsilon\varsigma}{\mathscr{AB}(\upsilon)\Gamma(\upsilon)} \int_0^t (t-\zeta)^{\upsilon-1}\zeta^{\varsigma-1} \left\| \mathrm{H}_1(\zeta,S) - \mathrm{H}_1(\zeta,S^\bullet) \right\| d\zeta \\ &\quad + \frac{\varsigma(1-\upsilon)t^{\varsigma-1}}{\mathscr{AB}(\upsilon)} \left\| \mathrm{H}_1(t,S) - \mathrm{H}_1(t,S^\bullet) \right\| \\ &\leq \left[\frac{\upsilon\varsigma\Gamma(\varsigma)}{\mathscr{AB}(\upsilon)\Gamma(\upsilon+\varsigma)} + \frac{\varsigma(1-\upsilon)}{\mathscr{AB}(\upsilon)} \right] \chi_1 \left\| S - S^\bullet \right\|. \end{aligned}$$

Let

$$\varpi_1 = \left[\frac{\upsilon\varsigma\Gamma(\varsigma)}{\mathscr{AB}(\upsilon)\Gamma(\upsilon+\varsigma)} + \frac{\varsigma(1-\upsilon)}{\mathscr{AB}(\upsilon)} \right] \left\| S - S^\bullet \right\|,$$

we get

$$\left\| S(t) - S^\bullet(t) \right\| \leq \chi_1\varpi_1.$$

Similarly, we have

$$\begin{aligned} \left\| Q(t) - Q^\bullet(t) \right\| &\leq \chi_2\varpi_2, \\ \left\| E(t) - E^\bullet(t) \right\| &\leq \chi_3\varpi_3, \\ \left\| I_h(t) - I_h^\bullet(t) \right\| &\leq \chi_4\varpi_4, \\ \left\| I(t) - I^\bullet(t) \right\| &\leq \chi_5\varpi_5, \\ \left\| R(t) - R^\bullet(t) \right\| &\leq \chi_6\varpi_6, \\ \left\| P(t) - P^\bullet(t) \right\| &\leq \chi_7\varpi_7. \end{aligned}$$

Theorem 6.1 *Proposed system (8) is HU stable assuming the aforementioned premises are true.*

Proof We comprehend that the Proposed system (8) has a unique solution if $S^{\bullet}(t)$, $Q^{\bullet}(t)$, $E^{\bullet}(t)$, $I_h^{\bullet}(t)$, $I^{\bullet}(t)$, $R^{\bullet}(t)$, $P^{\bullet}(t)$ be the approximate solution of model (8) that satisfies the model's requirements, then we get

$$
\begin{aligned}
\left\| S(t) - S^{\bullet}(t) \right\| &= \frac{\upsilon\varsigma}{\mathscr{A}\mathscr{B}(\upsilon)\Gamma(\upsilon)} \int_0^t (t-\zeta)^{\upsilon-1}\zeta^{\varsigma-1} \left\| \mathrm{H}_1(\zeta, S) - \mathrm{H}_1(\zeta, S^{\bullet}) \right\| d\zeta \\
&\quad + \frac{\varsigma(1-\upsilon)t^{\varsigma-1}}{\mathscr{A}\mathscr{B}(\upsilon)} \left\| \mathrm{H}_1(t, S) - \mathrm{H}_1(t, S^{\bullet}) \right\| \\
&\leq \left[\frac{\upsilon\varsigma\Gamma(\varsigma)}{\mathscr{A}\mathscr{B}(\upsilon)\Gamma(\upsilon+\varsigma)} + \frac{\varsigma(1-\upsilon)}{\mathscr{A}\mathscr{B}(\upsilon)} \right] \ell_1 \left\| S - S^{\bullet} \right\|, \\
o_1 &= \left[\frac{\upsilon\varsigma\Gamma(\varsigma)}{\mathscr{A}\mathscr{B}(\upsilon)\Gamma(\upsilon+\varsigma)} + \frac{\varsigma(1-\upsilon)}{\mathscr{A}\mathscr{B}(\upsilon)} \right] \left\| S - S^{\bullet} \right\|,
\end{aligned}
$$

$\wp_1 = \ell_1$, the aforementioned inequalities become

$$\left\| S(t) - S^{\bullet}(t) \right\| \leq o_1\wp_1.$$

Similarly

$$
\begin{aligned}
\left\| Q(t) - Q^{\bullet}(t) \right\| &\leq o_2\wp_2, \\
\left\| E(t) - E^{\bullet}(t) \right\| &\leq o_3\wp_3, \\
\left\| I_h(t) - I_h^{\bullet}(t) \right\| &\leq o_4\wp_4, \\
\left\| I(t) - I^{\bullet}(t) \right\| &\leq o_5\wp_5, \\
\left\| R(t) - R^{\bullet}(t) \right\| &\leq o_6\wp_6, \\
\left\| P(t) - P^{\bullet}(t) \right\| &\leq o_7\wp_7.
\end{aligned}
$$

this completes the proof that the COVID-19 model (8) is, by definition, hyers-ulams stable. □

7 Numerical scheme

To numerically solve the model (8), we describe a numerical technique [7] based on a Newton polynomial in this section. We write the equation (8) as follows for simplicity:

$$
\begin{aligned}
{}_0^{FFM}D_t^{\upsilon,\varsigma} S(t) &= S_1(t, S, Q, E, I_h, I, R, P), \\
{}_0^{FFM}D_t^{\upsilon,\varsigma} Q(t) &= Q_1(t, S, Q, E, I_h, I, R, P), \\
{}_0^{FFM}D_t^{\upsilon,\varsigma} E(t) &= E_1(t, S, Q, E, I_h, I, R, P) \\
{}_0^{FFM}D_t^{\upsilon,\varsigma} I_h(t) &= I_{h1}(t, S, Q, E, I_h, I, R, P), \\
{}_0^{FFM}D_t^{\upsilon,\varsigma} I(t) &= I_1(t, S, Q, E, I_h, I, R, P),
\end{aligned}
$$

$$
\begin{aligned}
{}_{0}^{FFM}D_t^{\upsilon,\varsigma}R(t) &= R_1(t,S,Q,E,I_h,I,R,P),\\
{}_{0}^{FFM}D_t^{\upsilon,\varsigma}P(t) &= P_1(t,S,Q,E,I_h,I,R,P).
\end{aligned}
\tag{14}
$$

The following results are obtained by using a fractal-fractional integral with the Mittag-Leffler kernel at the point $t_{k+1} = (k+1)\Delta t$.

$$
\begin{aligned}
S(t_{k+1}) = {} & \tfrac{1-\upsilon}{\mathscr{AB}(\upsilon)} t_k^{\varsigma-1} S_1(t_k, S(t_k), Q(t_k), E(t_k), I_h(t_k), I(t_k), R(t_k), P(t_k))\\
& + \tfrac{\upsilon}{\mathscr{AB}(\upsilon)\Gamma(\upsilon)} \sum_{\nu=2}^{k} \int_{t_\nu}^{t_{\nu+1}} S_1(t,S,Q,E,I_h,I,R,P)\zeta^{\varsigma-1}(t_{k+1}-\zeta)^{\upsilon-1}d\zeta,
\end{aligned}
\tag{15}
$$

$$
\begin{aligned}
Q(t_{k+1}) = {} & \tfrac{1-\upsilon}{\mathscr{AB}(\upsilon)} t_k^{\varsigma-1} Q_1(t_k, S(t_k), Q(t_k), E(t_k), I_h(t_k), I(t_k), R(t_k), P(t_k))\\
& + \tfrac{\upsilon}{\mathscr{AB}(\upsilon)\Gamma(\upsilon)} \sum_{\nu=2}^{k} \int_{t_\nu}^{t_{\nu+1}} Q_1(t,S,Q,E,I_h,I,R,P)\zeta^{\varsigma-1}(t_{k+1}-\zeta)^{\upsilon-1}d\zeta,
\end{aligned}
\tag{16}
$$

$$
\begin{aligned}
E(t_{k+1}) = {} & \tfrac{1-\upsilon}{\mathscr{AB}(\upsilon)} t_k^{\varsigma-1} E_1(t_k, S(t_k), Q(t_k), E(t_k), I_h(t_k), I(t_k), R(t_k), P(t_k))\\
& + \tfrac{\upsilon}{\mathscr{AB}(\upsilon)\Gamma(\upsilon)} \sum_{\nu=2}^{k} \int_{t_\nu}^{t_{\nu+1}} E_1(t,S,Q,E,I_h,I,R,P)\zeta^{\varsigma-1}(t_{k+1}-\zeta)^{\upsilon-1}d\zeta,
\end{aligned}
\tag{17}
$$

$$
\begin{aligned}
I_h(t_{k+1}) = {} & \tfrac{1-\upsilon}{\mathscr{AB}(\upsilon)} t_k^{\varsigma-1} I_{h_1}(t_k, S(t_k), Q(t_k), E(t_k), I_h(t_k), I(t_k), R(t_k), P(t_k))\\
& + \tfrac{\upsilon}{\mathscr{AB}(\upsilon)\Gamma(\upsilon)} \sum_{\nu=2}^{k} \int_{t_\nu}^{t_{\nu+1}} I_{h_1}(t,S,Q,E,I_h,I,R,P)\zeta^{\varsigma-1}(t_{k+1}-\zeta)^{\upsilon-1}d\zeta,
\end{aligned}
\tag{18}
$$

$$
\begin{aligned}
I(t_{k+1}) = {} & \tfrac{1-\upsilon}{\mathscr{AB}(\upsilon)} t_k^{\varsigma-1} I_1(t_k, S(t_k), Q(t_k), E(t_k), I_k(t_k), I(t_k), R(t_k), P(t_k))\\
& + \tfrac{\upsilon}{\mathscr{AB}(\upsilon)\Gamma(\upsilon)} \sum_{\nu=2}^{k} \int_{t_\nu}^{t_{\nu+1}} I_1(t,S,Q,E,I_h,I,R,P)\zeta^{\varsigma-1}(t_{k+1}-\zeta)^{\upsilon-1}d\zeta,
\end{aligned}
\tag{19}
$$

$$
\begin{aligned}
R(t_{k+1}) = {} & \tfrac{1-\upsilon}{\mathscr{AB}(\upsilon)} t_k^{1-\varsigma} R_1(t_k, S(t_k), Q(t_k), E(t_k), I_h(t_k), I(t_k), R(t_k), P(t_k))\\
& + \tfrac{\upsilon}{\mathscr{AB}(\upsilon)\Gamma(\upsilon)} \sum_{\nu=2}^{k} \int_{t_\nu}^{t_{\nu+1}} R_1(t,S,Q,E,I_h,I,R,P)\zeta^{\varsigma-1}(t_{k+1}-\zeta)^{\upsilon-1}d\zeta,
\end{aligned}
\tag{20}
$$

$$
\begin{aligned}
P(t_{k+1}) = {} & \tfrac{1-\upsilon}{\mathscr{AB}(\upsilon)} t_k^{\varsigma-1} P_1(t_k, S(t_k), Q(t_k), E(t_k), I_h(t_k), I(t_k), R(t_k), P(t_k))\\
& + \tfrac{\upsilon}{\mathscr{AB}(\upsilon)\Gamma(\upsilon)} \sum_{\nu=2}^{k} \int_{t_\nu}^{t_{\nu+1}} P_1(t,S,Q,E,I_h,I,R,P)\zeta^{\varsigma-1}(t_{k+1}-\zeta)^{\upsilon-1}d\zeta.
\end{aligned}
\tag{21}
$$

With the help of Newton's polynomial, we get

$$
\begin{aligned}
& G(t,S,Q,E,I_h,I,R,P)\\
& \quad \simeq G(t_{\nu-2}, S^{\nu-2}, Q^{\nu-2}, E^{\nu-2}, I_h^{\nu-2}, I^{\nu-2}, R^{\nu-2}, P^{\nu-2})
\end{aligned}
$$

$$
\begin{aligned}
&+ \frac{1}{\Delta t}(G(t_{\nu-1}, S^{\nu-1}, Q^{\nu-1}, E^{\nu-1}, I_h^{\nu-1}, I^{\nu-1}, R^{\nu-1}, P^{\nu-1}) \\
&- G(t_{\nu-2}, S^{\nu-2}, Q^{\nu-2}, E^{\nu-2}, I_h^{\nu-2}, I^{\nu-2}, R^{\nu-2}, P^{\nu-2}))(\varsigma - t_{\nu-2}) \\
&+ \frac{1}{2\Delta t^2}[G(t_\nu, S^\nu, Q^\nu, E^\nu, I_h^\nu, I^\nu, R^\nu, P^\nu) \\
&- 2G(t_{\nu-1}, S^{\nu-1}, Q^{\nu-1}, E^{\nu-1}, I_h^{\nu-1}, I^{\nu-1}, R^{\nu-1}, P^{\nu-1}) \\
&- G(t_{\nu-2}, S^{\nu-2}, Q^{\nu-2}, E^{\nu-2}, I_h^{\nu-2}, I^{\nu-2}, R^{\nu-2}, P^{\nu-2})] \\
&\times (\varsigma - t_{\nu-2})(\varsigma - t_{\nu-1}).
\end{aligned}
\tag{22}
$$

Replace the Newton polynomial above, we have

$$
\begin{aligned}
S^{(k+1)} =& \frac{\varsigma(1-\upsilon)}{\mathscr{A}\mathscr{B}(\upsilon)} t_k^{\varsigma-1} S_1(t_k, S^k, Q^k, E^k, I_h^k, I^k, R^k, P^k) \\
&+ \frac{\upsilon}{\mathscr{A}\mathscr{B}(\upsilon)\Gamma(\upsilon)} \sum_{\nu=2}^{k} S_1(t_{\nu-2}, \mathscr{P}_2) t_{\nu-2}^{\varsigma-1} \times \int_{t_\nu}^{t_{\nu+1}} (t_{k+1}-\tau)^{\upsilon-1} d\tau \\
&+ \frac{\upsilon}{\mathscr{A}\mathscr{B}(\upsilon_1)\Gamma(\upsilon)} \sum_{\nu=2}^{k} \frac{1}{\Delta t}\Big[t_{\nu-1}^{\varsigma-1} \;\; S_1(t_{\nu-1}, \mathscr{P}_1) \\
&- t_{\nu-2}^{1-\varsigma} \;\; S_1(t_{\nu-2}, \mathscr{P}_2)\Big] \times \int_{t_\nu}^{t_{\nu+1}} (\tau - t_{\nu-2})(t_{k+1}-\tau)^{\upsilon-1} d\tau \;\; + \\
&\frac{\upsilon_1}{\mathscr{A}\mathscr{B}(\upsilon_1)\Gamma(\upsilon)} \sum_{\nu=2}^{k} \frac{1}{2\Delta t^2}\Big[t_\nu^{\varsigma-1} S_1(t_\nu, \mathscr{P}) - 2t_{\nu-1}^{\varsigma-1} S_1(t_{\nu-1}, \mathscr{P}_1) \\
&+ t_{\nu-2}^{\varsigma-1} S_1(t_{\nu-2}, \mathscr{P}_2)\Big] \times \int_{t_\nu}^{t_{\nu+1}} (\tau - t_{\nu-2})(\tau - t_{\nu-1})(t_{k+1}-\tau)^{\upsilon-1} d\tau, \\
Q^{(k+1)} =& \frac{\varsigma(1-\upsilon)}{\mathscr{A}\mathscr{B}(\upsilon)} t_k^{\varsigma-1} Q_1(t_k, S^k, Q^k, E^k, I_h^k, I^k, R^k, P^k) \\
&+ \frac{\upsilon}{\mathscr{A}\mathscr{B}(\upsilon)\Gamma(\upsilon)} \sum_{\nu=2}^{k} Q_1(t_{\nu-2}, \mathscr{P}_2) t_{\nu-2}^{\varsigma-1} \times \int_{t_\nu}^{t_{\nu+1}} (t_{k+1}-\tau)^{\upsilon-1} d\tau \\
&+ \frac{\upsilon}{\mathscr{A}\mathscr{B}(\upsilon_1)\Gamma(\upsilon)} \sum_{\nu=2}^{k} \frac{1}{\Delta t}\Big[t_{\nu-1}^{\varsigma-1} \;\; Q_1(t_{\nu-1}, \mathscr{P}_1) \\
&- t_{\nu-2}^{1-\varsigma} \;\; Q_1(t_{\nu-2}, \mathscr{P}_2)\Big] \times \int_{t_\nu}^{t_{\nu+1}} (\tau - t_{\nu-2})(t_{k+1}-\tau)^{\upsilon-1} d\tau \;\; + \\
&\frac{\upsilon_1}{\mathscr{A}\mathscr{B}(\upsilon_1)\Gamma(\upsilon)} \sum_{\nu=2}^{k} \frac{1}{2\Delta t^2}\Big[t_\nu^{\varsigma-1} Q_1(t_\nu, \mathscr{P}) - 2t_{\nu-1}^{\varsigma-1} Q_1(t_{\nu-1}, \mathscr{P}_1) \\
&+ t_{\nu-2}^{\varsigma-1} Q_1(t_{\nu-2}, \mathscr{P}_2)\Big] \times \int_{t_\nu}^{t_{\nu+1}} (\tau - t_{\nu-2})(\tau - t_{\nu-1})(t_{k+1}-\tau)^{\upsilon-1} d\tau,
\end{aligned}
$$

$$
\begin{aligned}
E^{(k+1)} =& \frac{\varsigma(1-\upsilon)}{\mathscr{A}\mathscr{B}(\upsilon)} t_k^{\varsigma-1} E_1(t_k, S^k, Q^k, E^k, I_h^k, I^k, R^k, P^k) \\
& + \frac{\upsilon}{\mathscr{A}\mathscr{B}(\upsilon)\Gamma(\upsilon)} \sum_{\nu=2}^{k} E_1(t_{\nu-2}, \mathscr{P}_2) t_{\nu-2}^{\varsigma-1} \times \int_{t_\nu}^{t_{\nu+1}} (t_{k+1}-\tau)^{\upsilon-1} d\tau \\
& + \frac{\upsilon}{\mathscr{A}\mathscr{B}(\upsilon_1)\Gamma(\upsilon)} \sum_{\nu=2}^{k} \frac{1}{\Delta t} \Big[t_{\nu-1}^{\varsigma-1} \;\; E_1(t_{\nu-1}, \mathscr{P}_1) \\
& - t_{\nu-2}^{1-\varsigma} \;\; E_1(t_{\nu-2}, \mathscr{P}_2) \Big] \times \int_{t_\nu}^{t_{\nu+1}} (\tau - t_{\nu-2})(t_{k+1}-\tau)^{\upsilon-1} d\tau \;\; + \\
& \frac{\upsilon_1}{\mathscr{A}\mathscr{B}(\upsilon_1)\Gamma(\upsilon)} \sum_{\nu=2}^{k} \frac{1}{2\Delta t^2} \Big[t_\nu^{\varsigma-1} E_1(t_\nu, \mathscr{P}) - 2 t_{\nu-1}^{\varsigma-1} E_1(t_{\nu-1}, \mathscr{P}_1) \\
& + t_{\nu-2}^{\varsigma-1} E_1(t_{\nu-2}, \mathscr{P}_2) \Big] \times \int_{t_\nu}^{t_{\nu+1}} (\tau - t_{\nu-2})(\tau - t_{\nu-1})(t_{k+1}-\tau)^{\upsilon-1} d\tau, \\
I_h^{(k+1)} =& \frac{\varsigma(1-\upsilon)}{\mathscr{A}\mathscr{B}(\upsilon)} t_k^{\varsigma-1} I_{h_1}(t_k, S^k, Q^k, E^k, I_h^k, I^k, R^k, P^k) \\
& + \frac{\upsilon}{\mathscr{A}\mathscr{B}(\upsilon)\Gamma(\upsilon)} \sum_{\nu=2}^{k} I_{h_1}(t_{\nu-2}, \mathscr{P}_2) t_{\nu-2}^{\varsigma-1} \times \int_{t_\nu}^{t_{\nu+1}} (t_{k+1}-\tau)^{\upsilon-1} d\tau \\
& + \frac{\upsilon}{\mathscr{A}\mathscr{B}(\upsilon_1)\Gamma(\upsilon)} \sum_{\nu=2}^{k} \frac{1}{\Delta t} \Big[t_{\nu-1}^{\varsigma-1} \;\; I_{h_1}(t_{\nu-1}, \mathscr{P}_1) \\
& - t_{\nu-2}^{1-\varsigma} \;\; I_{h_1}(t_{\nu-2}, \mathscr{P}_2) \Big] \times \int_{t_\nu}^{t_{\nu+1}} (\tau - t_{\nu-2})(t_{k+1}-\tau)^{\upsilon-1} d\tau \;\; + \\
& \frac{\upsilon_1}{\mathscr{A}\mathscr{B}(\upsilon_1)\Gamma(\upsilon)} \sum_{\nu=2}^{k} \frac{1}{2\Delta t^2} \Big[t_\nu^{\varsigma-1} I_{h_1}(t_\nu, \mathscr{P}) - 2 t_{\nu-1}^{\varsigma-1} I_{h_1}(t_{\nu-1}, \mathscr{P}_1) \\
& + t_{\nu-2}^{\varsigma-1} I_{h_1}(t_{\nu-2}, \mathscr{P}_2) \Big] \times \int_{t_\nu}^{t_{\nu+1}} (\tau - t_{\nu-2})(\tau - t_{\nu-1})(t_{k+1}-\tau)^{\upsilon-1} d\tau,
\end{aligned}
$$

$$\begin{aligned}
I^{(k+1)} =& \frac{\varsigma(1-\upsilon)}{\mathscr{A}\mathscr{B}(\upsilon)} t_k^{\varsigma-1} I_1(t_k, S^k, Q^k, E^k, I_h^k, I^k, R^k, P^k) \\
&+ \frac{\upsilon}{\mathscr{A}\mathscr{B}(\upsilon)\Gamma(\upsilon)} \sum_{\nu=2}^{k} I_1(t_{\nu-2}, \mathscr{P}_2) t_{\nu-2}^{\varsigma-1} \times \int_{t_\nu}^{t_{\nu+1}} (t_{k+1}-\tau)^{\upsilon-1} d\tau \\
&+ \frac{\upsilon}{\mathscr{A}\mathscr{B}(\upsilon_1)\Gamma(\upsilon)} \sum_{\nu=2}^{k} \frac{1}{\Delta t} \Big[t_{\nu-1}^{\varsigma-1} \;\; I_1(t_{\nu-1}, \mathscr{P}_1) \\
&- t_{\nu-2}^{1-\varsigma} \;\; I_1(t_{\nu-2}, \mathscr{P}_2) \Big] \times \int_{t_\nu}^{t_{\nu+1}} (\tau - t_{\nu-2})(t_{k+1}-\tau)^{\upsilon-1} d\tau \;\; + \\
&\frac{\upsilon_1}{\mathscr{A}\mathscr{B}(\upsilon_1)\Gamma(\upsilon)} \sum_{\nu=2}^{k} \frac{1}{2\Delta t^2} \Big[t_\nu^{\varsigma-1} I_1(t_\nu, \mathscr{P}) - 2t_{\nu-1}^{\varsigma-1} I_1(t_{\nu-1}, \mathscr{P}_1) \\
&+ t_{\nu-2}^{\varsigma-1} I_1(t_{\nu-2}, \mathscr{P}_2) \Big] \times \int_{t_\nu}^{t_{\nu+1}} (\tau - t_{\nu-2})(\tau - t_{\nu-1})(t_{k+1}-\tau)^{\upsilon-1} d\tau, \\
R^{(k+1)} =& \frac{\varsigma(1-\upsilon)}{\mathscr{A}\mathscr{B}(\upsilon)} t_k^{\varsigma-1} R_1(t_k, S^k, Q^k, E^k, I_h^k, I^k, R^k, P^k) \\
&+ \frac{\upsilon}{\mathscr{A}\mathscr{B}(\upsilon)\Gamma(\upsilon)} \sum_{\nu=2}^{k} R_1(t_{\nu-2}, \mathscr{P}_2) t_{\nu-2}^{\varsigma-1} \times \int_{t_\nu}^{t_{\nu+1}} (t_{k+1}-\tau)^{\upsilon-1} d\tau \\
&+ \frac{\upsilon}{\mathscr{A}\mathscr{B}(\upsilon_1)\Gamma(\upsilon)} \sum_{\nu=2}^{k} \frac{1}{\Delta t} \Big[t_{\nu-1}^{\varsigma-1} \;\; R_1(t_{\nu-1}, \mathscr{P}_1) \\
&- t_{\nu-2}^{1-\varsigma} \;\; R_1(t_{\nu-2}, \mathscr{P}_2) \Big] \times \int_{t_\nu}^{t_{\nu+1}} (\tau - t_{\nu-2})(t_{k+1}-\tau)^{\upsilon-1} d\tau \;\; + \\
&\frac{\upsilon_1}{\mathscr{A}\mathscr{B}(\upsilon_1)\Gamma(\upsilon)} \sum_{\nu=2}^{k} \frac{1}{2\Delta t^2} \Big[t_\nu^{\varsigma-1} R_1(t_\nu, \mathscr{P}) - 2t_{\nu-1}^{\varsigma-1} R_1(t_{\nu-1}, \mathscr{P}_1) \\
&+ t_{\nu-2}^{\varsigma-1} R_1(t_{\nu-2}, \mathscr{P}_2) \Big] \times \int_{t_\nu}^{t_{\nu+1}} (\tau - t_{\nu-2})(\tau - t_{\nu-1})(t_{k+1}-\tau)^{\upsilon-1} d\tau,
\end{aligned}$$

$$
\begin{aligned}
P^{(k+1)} =&\frac{\varsigma(1-\upsilon)}{\mathscr{A}\mathscr{B}(\upsilon)} t_k^{\varsigma-1} P_1(t_k, S^k, Q^k, E^k, I_h^k, I^k, R^k, P^k)\\
&+ \frac{\upsilon}{\mathscr{A}\mathscr{B}(\upsilon)\Gamma(\upsilon)} \sum_{\nu=2}^{k} P_1(t_{\nu-2}, \mathscr{P}_2) t_{\nu-2}^{\varsigma-1} \times \int_{t_\nu}^{t_{\nu+1}} (t_{k+1}-\tau)^{\upsilon-1} d\tau\\
&+ \frac{\upsilon}{\mathscr{A}\mathscr{B}(\upsilon_1)\Gamma(\upsilon)} \sum_{\nu=2}^{k} \frac{1}{\Delta t} \Big[t_{\nu-1}^{\varsigma-1} \;\; P_1(t_{\nu-1}, \mathscr{P}_1)\\
&- t_{\nu-2}^{1-\varsigma} \;\; P_1(t_{\nu-2}, \mathscr{P}_2)\Big] \times \int_{t_\nu}^{t_{\nu+1}} (\tau - t_{\nu-2})(t_{k+1}-\tau)^{\upsilon-1} d\tau \;\; +\\
&\frac{\upsilon_1}{\mathscr{A}\mathscr{B}(\upsilon_1)\Gamma(\upsilon)} \sum_{\nu=2}^{k} \frac{1}{2\Delta t^2} \Big[t_\nu^{\varsigma-1} P_1(t_\nu, \mathscr{P}) - 2 t_{\nu-1}^{\varsigma-1} P_1(t_{\nu-1}, \mathscr{P}_1)\\
&+ t_{\nu-2}^{\varsigma-1} P_1(t_{\nu-2}, \mathscr{P}_2)\Big] \times \int_{t_\nu}^{t_{\nu+1}} (\tau - t_{\nu-2})(\tau - t_{\nu-1})(t_{k+1}-\tau)^{\upsilon-1} d\tau,
\end{aligned}
$$

where

$$
\begin{aligned}
\mathscr{P} &= S^\nu, Q^\nu, E^\nu, I_h^\nu, I^\nu, R^\nu, P^\nu,\\
\mathscr{P}_1 &= S^{\nu-1}, Q^{\nu-1}, E^{\nu-1}, I_h^{\nu-1}, I^{\nu-1}, R^{\nu-1}, P^{\nu-1},\\
\mathscr{P}_2 &= S^{\nu-2}, Q^{\nu-2}, E^{\nu-2}, I_h^{\nu-2}, I^{\nu-2}, R^{\nu-2}, P^{\nu-2}.
\end{aligned}
$$

For integral in above equation, we can have the following values

$$
\begin{aligned}
\int_{t_\nu}^{t_{\nu+1}} (t_{\delta+1}-\tau)^{\upsilon-1} d\tau &=\frac{(\Delta t)^\upsilon}{\upsilon_1}\Big[\xi\Big],\\
\int_{t_\nu}^{t_{\nu+1}} (\tau - t_{\nu-2})(t_{\delta+1}-\tau)^{\upsilon-1} d\tau &=\frac{(\Delta t)^{\upsilon+1}}{\upsilon(\upsilon+1)}\Big[\xi_1\Big],\\
\int_{t_\nu}^{t_{\nu+1}} (\tau - t_{\nu-2})(\tau - t_{\nu-1})(t_{\delta+1}-\tau)^{\upsilon-1} d\tau &=\frac{(\Delta t)^{\upsilon+2}}{\upsilon(\upsilon+1)(\upsilon+2)} \times \Big[\xi_2\Big],
\end{aligned}
\tag{23}
$$

where

$$
\begin{aligned}
\xi &= (k-\nu+1)^\upsilon - (k-\nu)^\upsilon,\\
\xi_1 &= (k-\nu+1)^\upsilon (k-\nu+3+2\upsilon) - (k-\nu)^\upsilon (k-\nu+3+3\upsilon),\\
\xi_2 &= (k-\nu+1)^\upsilon \{2(k-\nu)^2 + (3\upsilon+10)(k-\nu) + 2\upsilon^2 + 9\upsilon + 12\}\\
&\quad -(k-\nu)^\upsilon \{2(k-\nu)^2 + (5\upsilon+10)(k-\nu) + 6\upsilon^2 + 18\upsilon + 12\}.
\end{aligned}
$$

Therefore, the numerical scheme for model (8) is as follows:

$$
\begin{aligned}
S^{(k+1)} =& \frac{1-\upsilon}{\mathscr{A}\mathscr{B}(\varsigma)} t_k^{\varsigma-1} S_1(t_k, S^k, Q^k, I_h^k, I^k, R^k, P^k) \\
&+ \frac{\upsilon(\Delta t)^{\upsilon}}{\mathscr{A}\mathscr{B}(\upsilon)\Gamma(\upsilon+1)} \sum_{\nu=2}^{k} t_{\nu-2}^{\varsigma-1} S_1(t_{\nu-2}, \mathscr{P}_2) \times \Big[\xi\Big] \\
&+ \frac{\upsilon(\Delta t)^{\upsilon}}{\mathscr{A}\mathscr{B}(\upsilon_1)\Gamma(\upsilon+2)} \sum_{\nu=2}^{k} \Big[t_{\nu-1}^{\varsigma-1} \ S_1(t_{\nu-1}, \mathscr{P}_1) \\
&- t_{\nu-2}^{\varsigma-1} \ S_1(t_{\nu-2}, \mathscr{P}_2)\Big] \times \Big[\xi_1\Big] \ + \frac{\upsilon(\Delta t)^{\upsilon}}{2\mathscr{A}\mathscr{B}(\upsilon)\Gamma(\upsilon+3)} \sum_{\nu=2}^{k} \Big[t_{\nu}^{\varsigma-1} S_1(t_{\nu}, \mathscr{P}) \\
&- 2t_{\nu-1}^{\varsigma-1} S_1(t_{\nu-1}, \mathscr{P}_1) + t_{\nu-2}^{\varsigma-1} S_1(t_{\nu-2}, \mathscr{P}_2)\Big] \times \Big[\xi_2\Big]. \\
Q^{(k+1)} =& \frac{1-\upsilon}{\mathscr{A}\mathscr{B}(\varsigma)} t_k^{\varsigma-1} Q_1(t_k, S^k, Q^k, I_h^k, I^k, R^k, P^k) \\
&+ \frac{\upsilon(\Delta t)^{\upsilon}}{\mathscr{A}\mathscr{B}(\upsilon)\Gamma(\upsilon+1)} \sum_{\nu=2}^{k} t_{\nu-2}^{\varsigma-1} Q_1(t_{\nu-2}, \mathscr{P}_2) \times \Big[\xi\Big] \\
&+ \frac{\upsilon(\Delta t)^{\upsilon}}{\mathscr{A}\mathscr{B}(\upsilon_1)\Gamma(\upsilon+2)} \sum_{\nu=2}^{k} \Big[t_{\nu-1}^{\varsigma-1} \ Q_1(t_{\nu-1}, \mathscr{P}_1) \\
&- t_{\nu-2}^{\varsigma-1} \ Q_1(t_{\nu-2}, \mathscr{P}_2)\Big] \times \Big[\xi_1\Big] \ + \frac{\upsilon(\Delta t)^{\upsilon}}{2\mathscr{A}\mathscr{B}(\upsilon)\Gamma(\upsilon+3)} \sum_{\nu=2}^{k} \Big[t_{\nu}^{\varsigma-1} Q_1(t_{\nu}, \mathscr{P}) \\
&- 2t_{\nu-1}^{\varsigma-1} Q_1(t_{\nu-1}, \mathscr{P}_1) + t_{\nu-2}^{\varsigma-1} Q_1(t_{\nu-2}, \mathscr{P}_2)\Big] \times \Big[\xi_2\Big], \\
E^{(k+1)} =& \frac{1-\upsilon}{\mathscr{A}\mathscr{B}(\varsigma)} t_k^{\varsigma-1} E_1(t_k, S^k, Q^k, I_h^k, I^k, R^k, P^k) \\
&+ \frac{\upsilon(\Delta t)^{\upsilon}}{\mathscr{A}\mathscr{B}(\upsilon)\Gamma(\upsilon+1)} \sum_{\nu=2}^{k} t_{\nu-2}^{\varsigma-1} E_1(t_{\nu-2}, \mathscr{P}_2) \times \Big[\xi\Big] \\
&+ \frac{\upsilon(\Delta t)^{\upsilon}}{\mathscr{A}\mathscr{B}(\upsilon_1)\Gamma(\upsilon+2)} \sum_{\nu=2}^{k} \Big[t_{\nu-1}^{\varsigma-1} \ E_1(t_{\nu-1}, \mathscr{P}_1) \\
&- t_{\nu-2}^{\varsigma-1} \ E_1(t_{\nu-2}, \mathscr{P}_2)\Big] \times \Big[\xi_1\Big] \ + \frac{\upsilon(\Delta t)^{\upsilon}}{2\mathscr{A}\mathscr{B}(\upsilon)\Gamma(\upsilon+3)} \sum_{\nu=2}^{k} \Big[t_{\nu}^{\varsigma-1} E_1(t_{\nu}, \mathscr{P}) \\
&- 2t_{\nu-1}^{\varsigma-1} E_1(t_{\nu-1}, \mathscr{P}_1) + t_{\nu-2}^{\varsigma-1} E_1(t_{\nu-2}, \mathscr{P}_2)\Big] \times \Big[\xi_2\Big],
\end{aligned}
$$

$$
\begin{aligned}
I_h^{(k+1)} =& \frac{1-\upsilon}{\mathscr{A}\mathscr{B}(\varsigma)} t_k^{\varsigma-1} I_{h_1}(t_k, S^k, Q^k, I_h^k, I^k, R^k, P^k) \\
&+ \frac{\upsilon(\Delta t)^{\upsilon}}{\mathscr{A}\mathscr{B}(\upsilon)\Gamma(\upsilon+1)} \sum_{\nu=2}^{k} t_{\nu-2}^{\varsigma-1} I_{h_1}(t_{\nu-2}, \mathscr{P}_2) \times \Big[\xi\Big] \\
&+ \frac{\upsilon(\Delta t)^{\upsilon}}{\mathscr{A}\mathscr{B}(\upsilon_1)\Gamma(\upsilon+2)} \sum_{\nu=2}^{k} \Big[t_{\nu-1}^{\varsigma-1} \;\; I_{h_1}(t_{\nu-1}, \mathscr{P}_1) \\
&- t_{\nu-2}^{\varsigma-1} \;\; S_1(t_{\nu-2}, \mathscr{P}_2)\Big] \times \Big[\xi_1\Big] \;\; + \frac{\upsilon(\Delta t)^{\upsilon}}{2\mathscr{A}\mathscr{B}(\upsilon)\Gamma(\upsilon+3)} \sum_{\nu=2}^{k} \Big[t_{\nu}^{\varsigma-1} I_{h_1}(t_{\nu}, \mathscr{P}) \\
&- 2t_{\nu-1}^{\varsigma-1} I_{h_1}(t_{\nu-1}, \mathscr{P}_1) + t_{\nu-2}^{\varsigma-1} I_{h_1}(t_{\nu-2}, \mathscr{P}_2)\Big] \times \Big[\xi_2\Big], \\
I^{(k+1)} =& \frac{1-\upsilon}{\mathscr{A}\mathscr{B}(\varsigma)} t_k^{\varsigma-1} I_1(t_k, S^k, Q^k, I_h^k, I^k, R^k, P^k) \\
&+ \frac{\upsilon(\Delta t)^{\upsilon}}{\mathscr{A}\mathscr{B}(\upsilon)\Gamma(\upsilon+1)} \sum_{\nu=2}^{k} t_{\nu-2}^{\varsigma-1} I_1(t_{\nu-2}, \mathscr{P}_2) \times \Big[\xi\Big] \\
&+ \frac{\upsilon(\Delta t)^{\upsilon}}{\mathscr{A}\mathscr{B}(\upsilon_1)\Gamma(\upsilon+2)} \sum_{\nu=2}^{k} \Big[t_{\nu-1}^{\varsigma-1} \;\; I_1(t_{\nu-1}, \mathscr{P}_1) \\
&- t_{\nu-2}^{\varsigma-1} \;\; I_1(t_{\nu-2}, \mathscr{P}_2)\Big] \times \Big[\xi_1\Big] \;\; + \frac{\upsilon(\Delta t)^{\upsilon}}{2\mathscr{A}\mathscr{B}(\upsilon)\Gamma(\upsilon+3)} \sum_{\nu=2}^{k} \Big[t_{\nu}^{\varsigma-1} I_1(t_{\nu}, \mathscr{P}) \\
&- 2t_{\nu-1}^{\varsigma-1} I_1(t_{\nu-1}, \mathscr{P}_1) + t_{\nu-2}^{\varsigma-1} I_1(t_{\nu-2}, \mathscr{P}_2)\Big] \times \Big[\xi_2\Big], \\
R^{(k+1)} =& \frac{1-\upsilon}{\mathscr{A}\mathscr{B}(\varsigma)} t_k^{\varsigma-1} R_1(t_k, S^k, Q^k, I_h^k, I^k, R^k, P^k) \\
&+ \frac{\upsilon(\Delta t)^{\upsilon}}{\mathscr{A}\mathscr{B}(\upsilon)\Gamma(\upsilon+1)} \sum_{\nu=2}^{k} t_{\nu-2}^{\varsigma-1} R_1(t_{\nu-2}, \mathscr{P}_2) \times \Big[\xi\Big] \\
&+ \frac{\upsilon(\Delta t)^{\upsilon}}{\mathscr{A}\mathscr{B}(\upsilon_1)\Gamma(\upsilon+2)} \sum_{\nu=2}^{k} \Big[t_{\nu-1}^{\varsigma-1} \;\; R_1(t_{\nu-1}, P_1) \\
&- t_{\nu-2}^{\varsigma-1} \;\; R_1(t_{\nu-2}, \mathscr{P}_2)\Big] \times \Big[\xi_1\Big] \;\; + \frac{\upsilon(\Delta t)^{\upsilon}}{2\mathscr{A}\mathscr{B}(\upsilon)\Gamma(\upsilon+3)} \sum_{\nu=2}^{k} \Big[t_{\nu}^{\varsigma-1} R_1(t_{\nu}, \mathscr{P}) \\
&- 2t_{\nu-1}^{\varsigma-1} R_1(t_{\nu-1}, \mathscr{P}_1) + t_{\nu-2}^{\varsigma-1} R_1(t_{\nu-2}, \mathscr{P}_2)\Big] \times \Big[\xi_2\Big],
\end{aligned}
$$

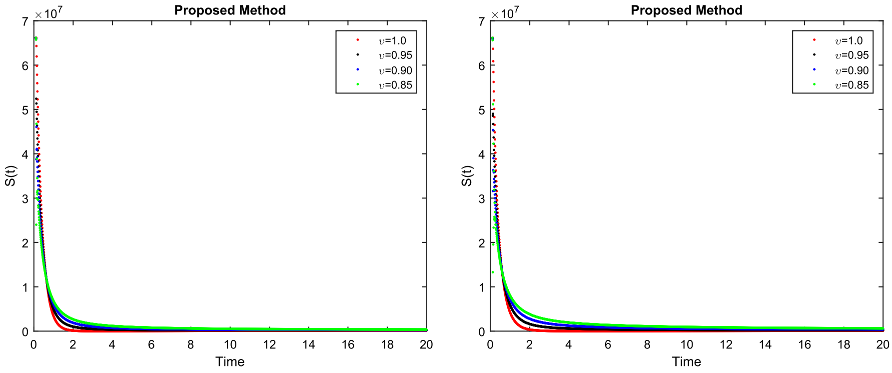

(a) (b)

Fig. 1 Simulation of S:(a) When the fractal dimension is $\varsigma = 1$ for various fractional orders of υ. (b) When the fractal dimension is $\varsigma = 0.8$ for different fractional orders of υ

$$\begin{aligned} P^{(k+1)} =& \frac{1-\upsilon}{\mathscr{AB}(\varsigma)} t_k^{\varsigma-1} P_1(t_k, S^k, Q^k, I_h^k, I^k, R^k, P^k) \\ &+ \frac{\upsilon(\Delta t)^{\upsilon}}{\mathscr{AB}(\upsilon)\Gamma(\upsilon+1)} \sum_{\nu=2}^{k} t_{\nu-2}^{\varsigma-1} P_1(t_{\nu-2}, \mathscr{P}_2) \times \Big[\xi\Big] \\ &+ \frac{\upsilon(\Delta t)^{\upsilon}}{\mathscr{AB}(\upsilon_1)\Gamma(\upsilon+2)} \sum_{\nu=2}^{k} \Big[t_{\nu-1}^{\varsigma-1} \; S_1(t_{\nu-1}, \mathscr{P}_1) \\ &- t_{\nu-2}^{\varsigma-1} \; P_1(t_{\nu-2}, \mathscr{P}_2)\Big] \times \Big[\xi_1\Big] + \frac{\upsilon(\Delta t)^{\upsilon}}{2\mathscr{AB}(\upsilon)\Gamma(\upsilon+3)} \sum_{\nu=2}^{k} \Big[t_{\nu}^{\varsigma-1} P_1(t_\nu, \mathscr{P}) \\ &- 2t_{\nu-1}^{\varsigma-1} P_1(t_{\nu-1}, \mathscr{P}_1) + t_{\nu-2}^{\varsigma-1} P_1(t_{\nu-2}, \mathscr{P}_2)\Big] \times \Big[\xi_2\Big]. \end{aligned}$$

8 Numerical Simulations and Discussion

This section presents the graphical result of the model (8). Using a fractal-fractional differential operator of the Mittage-Leffler kernel with fractional-order $\upsilon(1, 0.95, 0.90, 0.85)$ and fractal dimensions ς (1, 0.8), the results are analyzed. MATLAB a computational software is used to perform simulations and compute the results using a numerical scheme. The parameter values obtained from article [8]are $A^{\upsilon} = 0.000028$, $\kappa^{\upsilon} = 0.000021$, $\sigma^{\upsilon} = 0.0397$, $\theta^{\upsilon} = 0.8$, $\alpha^{\upsilon} = 0.00414$, $\beta = 0.333333$, $\omega_1^{\upsilon} = 0.1$, $\omega_2^{\upsilon} = 0.1$, $\gamma_1^{\upsilon} = 1/5.2$, $\gamma_2^{\upsilon} = 1/5.2$, $\eta_1^{\upsilon} = 1/10$, $\eta_2^{\upsilon} = 1/10$, $\delta^{\upsilon} = 0.00011$, $\mu^{\upsilon} = 0.1$, $\kappa_p^{\upsilon} = 0.1724$, $m^{\upsilon} = 1/90$ and the initial values are $S(0) = 66170000$, $Q(0) = 12$, $E(0) = 6331$, $I_h = 0$, $I(0) = 0$, $R(0) = 0$, $P(0) = 500$. The susceptible population's dynamics rapidly decline over $0 - 1$ days, as shown in Figure (1). After exposure to the virus, this population decline shifts to populations in the incubation period, where population dynamics are divided into two

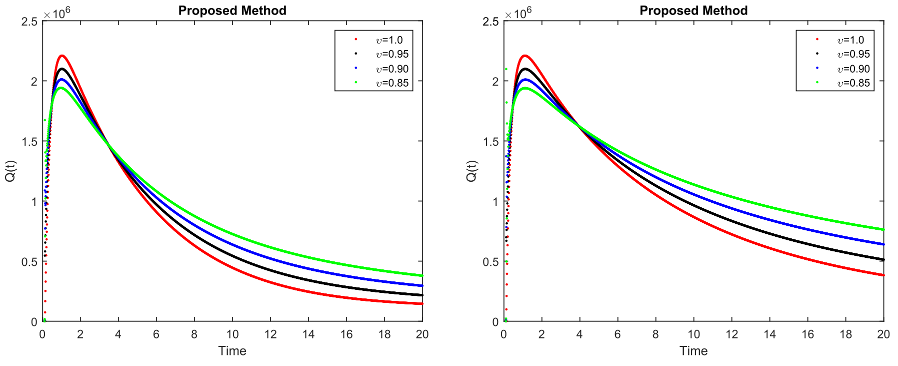

(a) (b)

Fig. 2 Simulation of Q:(a) When the fractal dimension is $\varsigma = 1$ for various fractional orders of υ. (b) When the fractal dimension is $\varsigma = 0.8$ for different fractional orders of υ

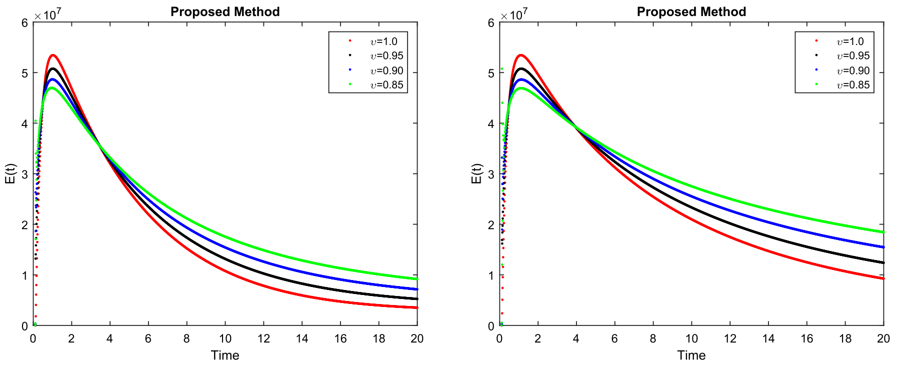

(a) (b)

Fig. 3 Simulation of E:(a) When the fractal dimension is $\varsigma = 1$ for various fractional orders of υ. (b) When the fractal dimension is $\varsigma = 0.8$ for different fractional orders of υ

classes: the quarantine class and the exposed class, as shown in Figures (2) and (3), respectively. The dynamics of the exposed class and the quarantine class increase rapidly over $0-2$ per day. After day 2, the dynamics of both classes decline rapidly. The dynamics of the exposed population and the hospitalized infected population are connected, respectively, to each other. Hospitalized infected population and infected population dynamics increase fast over $0-7$ days as a result of population changes during the incubation phase leading to the infected population, then rapidly drops after that. Figures (4) and (5) depict the dynamics of the hospitalized infected population and the infected population, respectively. In the recovered population dynamics, the last component of the human population dynamics is expressed. It increases gradually over $0-20$ days before starting to stabilize as shown in Figure (6). The infectious population contributes to a portion of the environmental pathogen population. Pathogen counts peak between 0 and 12 days, after which they start to decline. Figure (7) depicts

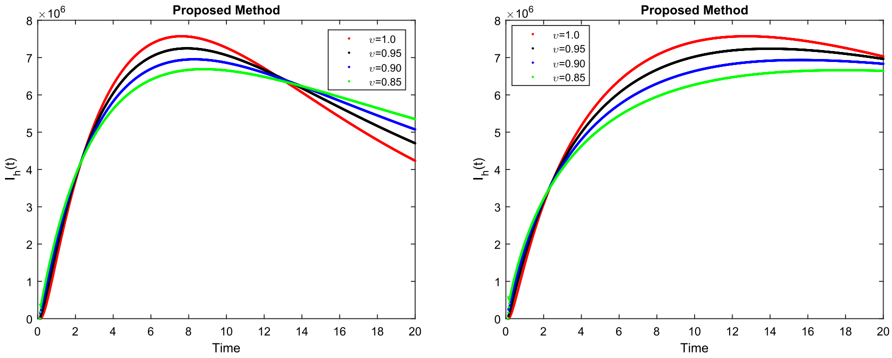

(a) (b)

Fig. 4 Simulation of I_h:(a) When the fractal dimension is $\varsigma = 1$ for various fractional orders of υ. (b) When the fractal dimension is $\varsigma = 0.8$ for different fractional orders of υ

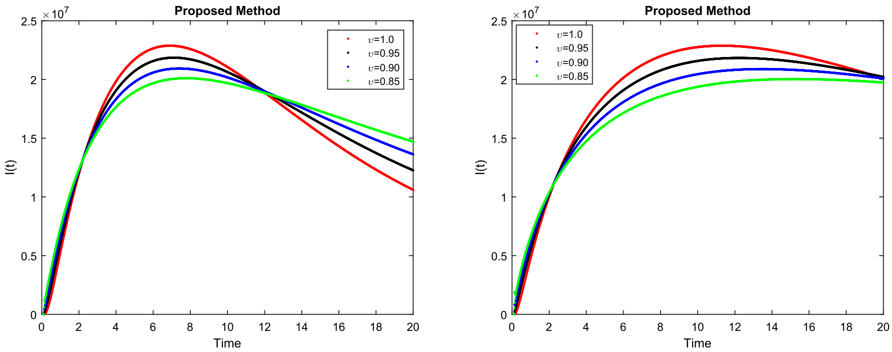

(a) (b)

Fig. 5 Simulation of I:(a) When the fractal dimension is $\varsigma = 1$ for various fractional orders of υ. (b) When the fractal dimension is $\varsigma = 0.8$ for different fractional orders of υ

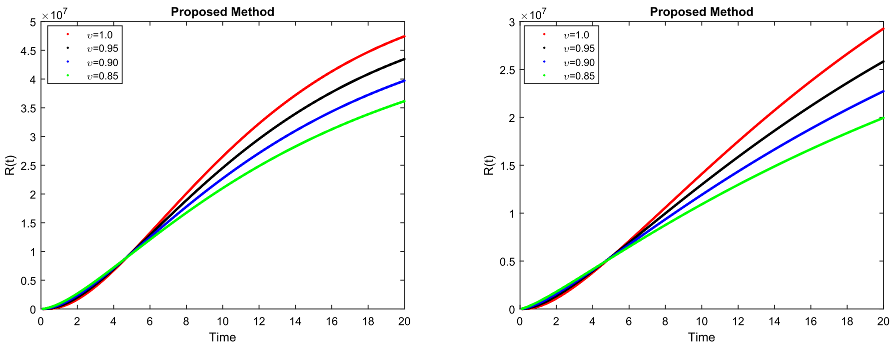

(a) (b)

Fig. 6 Simulation of R:(a) When the fractal dimension is $\varsigma = 1$ for various fractional orders of υ. (b) When the fractal dimension is $\varsigma = 0.8$ for different fractional orders of υ

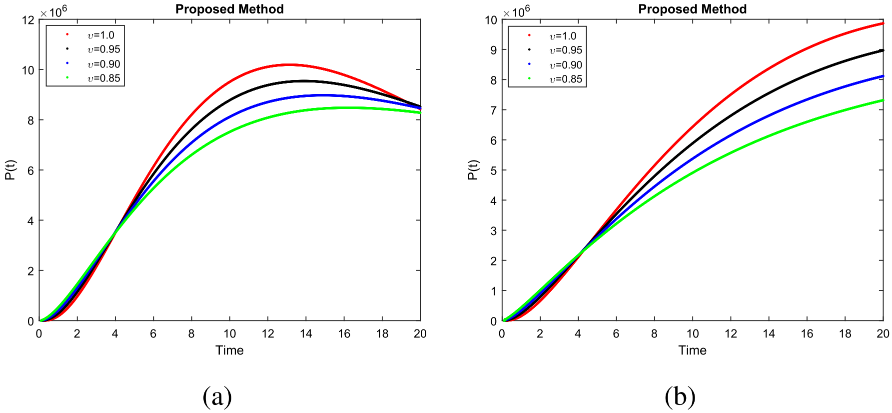

Fig. 7 Simulation of P.(a) When the fractal dimension is $\varsigma = 1$ and there are different fractional orders of υ. (b) When the fractal dimension is $\varsigma = 0.8$ for different fractional orders of υ

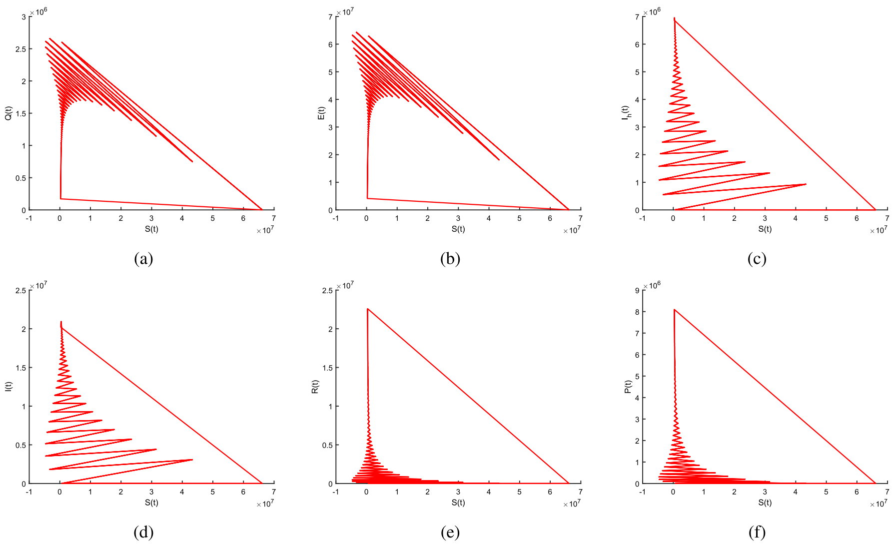

Fig. 8 Chaotic attractor of system (8) in different 2D-projections for $\upsilon = 0.9$. (a) SQ-Plan. (b) SE-Plan. (c)SI_h-Plan. (d) SI-Plan. (e) SR-Plan. (f) SP-Plan

the dynamics of the pathogen population. We have seen from the numerical findings that are shown in the graphs that the number of exposed and vulnerable individuals immediately decreases and moves into the infected class. The infection is under control while they remain under quarantine. After some duration, the recovery rate is increased by using control and treatment factors. This demonstrates the significance of quarantine in the management of infection.

Figures (1)-(11) illustrate the graphical representation of the impact of arbitrary fractional-order υ and the fractal dimension ς (memory index) on various population dynamics. In Figure (1)(a, b), it is evident that the susceptible population decreases to a specific positive density for all values of υ and ς. The decrease in the number of susceptible individuals is evident as the fractional order decreases. This reduction occurs because the fractional order enables a more precise depiction of the system's memory and hereditary characteristics, resulting in a closer alignment of the model with real-world data. Specifically, Figure (1)(a) depicting susceptible individuals with a fractal dimension of 1 ($\varsigma = 1.0$) exhibits behavior consistent with the standard epidemic model. In contrast, Figure (1)(b) representing a fractal dimension of 0.8 ($\varsigma = 0.8$) illustrates the influence of fractional-order effects on the dynamics of susceptible individuals. Figure (2)(a, b) illustrates the dynamics of quarantine individuals for varying υ and ς. It is observed that the quarantine population initially increases around t = 2 days and then slightly decreases to a specific positive density for all values of υ and ς. Examining how curves for different fractal orders react to quarantine provides insight into the effectiveness of these measures in containing the spread of COVID-19. A substantial decrease in the number of infected individuals following quarantine implementation suggests its beneficial impact on epidemic mitigation. Figure (3)(a, b) showcases the dynamics of exposed individuals across different values of υ and ς. It is noted that the peaks of the exposed curves decrease slightly and occur over a longer period for smaller values of υ and ς. Similarly, Figures (4)(a,b) and (5)(a,b) depict the dynamics of the hospitalized infected and infected classes, respectively. The peaks of these curves also decrease slightly and occur over extended periods for smaller values of υ and ς. A decrease in the fractal dimension affects the dynamics of infected individuals. The graphs might display a decline in the number of infected individuals as the fractional order decreases, indicating the model's enhanced accuracy in depicting disease spread with lower fractal dimensions. Figure (6) (a, b)analyzes the dynamics of the recovered or removed population across various υ and ς values. Initially, the curve depicting recovered individuals experiences a rise before reaching a stable level. The impact of the fractal dimension on recovered individuals is also noticeable. Lower fractal dimensions could result in alterations in the recovery dynamics, potentially influencing the speed at which individuals move from being infected to recovering. Figure (7)(a, b) analyzes the dynamics of the pathogen population across various υ and ς values. We observe that, for different values of υ, the model's solution continuously depends on the time-fractional derivative yet eventually reaches the equilibrium points.

We illustrated the chaotic attractors of the model (8) in Figures (8) - (11), which were produced using the FFM operator's numerical method for specific parameter values. The dynamics of the propagation of infectious diseases, such as COVID-19, are by nature nonlinear. This implies that even minor adjustments to the starting circumstances or parameters might greatly impact the final results. Scholars can better comprehend and visualize these intricate, nonlinear interactions with the aid of chaotic figures. COVID-19 models need to take into consideration a lot of variables that affect how diseases spread, such as the biology of the virus, human behavior, government actions, and the availability of healthcare. The Figures (8)(a-f) display the comparative chaotic behaviors between different groups: Figure (8)(a) shows the comparison between susceptible and quarantined individuals, Figure (8)(b) illustrates the comparison between susceptible and exposed individuals, Figure (8)(c) depicts the comparison between susceptible and hospitalized infected individuals, Figure (8)(d) shows the comparison between susceptible and infected individuals, Fig. 8(e)

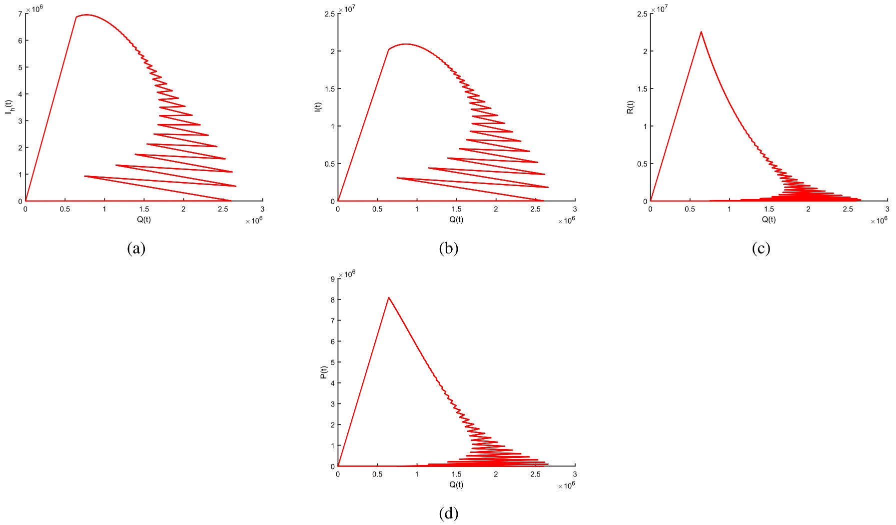

Fig. 9 Chaotic attractor of system (8) in different 2D-projections for $\upsilon = 0.9$. (a) QI_h-Plan. (b) QI-Plan. (c)QR-Plan. (d) QP-Plan

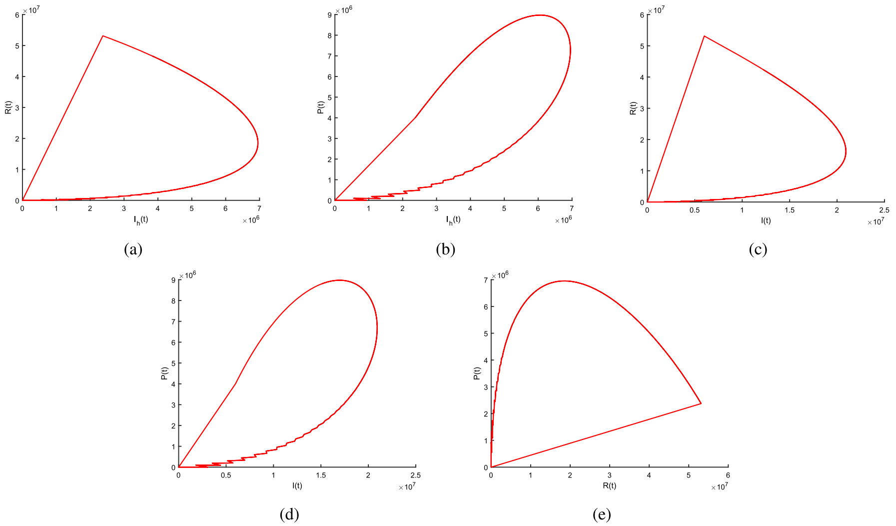

Fig. 10 Chaotic attractor of system (8) in different 2D-projections for $\upsilon = 0.9$. (a) $I_h R$-Plan. (b) $I_h P$-Plan. (c)IR-Plan. (d) IP-Plan. (e) RP-Plan

illustrates the comparison between susceptible and recovered individuals, and Figure (8)(f) displays the comparison between susceptible and pathogen individuals when $\upsilon = 0.9$. Figures (9)(a-d) display the comparative chaotic behaviors between different groups: Figure (9)(a) shows the comparison between quarantined and hospitalized infected individuals, Figure (9)(b) illustrates the comparison between quarantined and infected individuals, Figure (9)(c) depicts the comparison between quarantined and

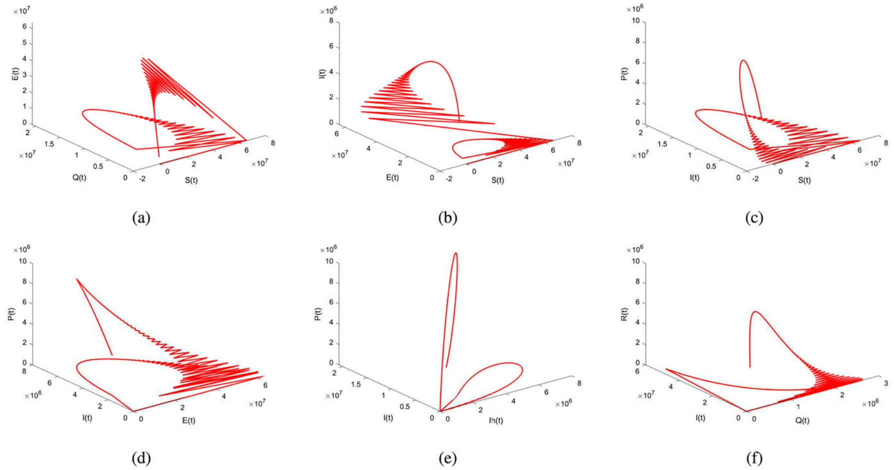

Fig. 11 Chaotic behavior of the different compartment in the feasible region for stable solution in domain

recovered individuals, and Figure (9)(d) displays the comparison between susceptible and pathogen individuals when $\upsilon = 0.9$. Figure (10)(a) shows the comparative chaotic behaviors between hospitalized infected and recovered individuals, while Figure (10)(b) illustrates the comparative chaotic behaviors between hospitalized infected and pathogen individuals when $\upsilon = 0.9$. The graph illustrates the chaotic and dynamic nature of an epidemic, highlighting the swift increase and decrease of hospitalized infected individuals followed by a subsequent rise in recoveries over time. This pattern emphasizes the intricate challenge of managing and controlling infectious diseases within a population. Figure (10)(c) depicts the comparative chaotic behaviors between infected and recovered individuals, while Figure (10)(d) illustrates the comparative chaotic behaviors between infected and pathogen individuals when $\upsilon = 0.9$. The graph illustrates the chaotic and dynamic nature of an epidemic, showcasing the rapid increase and decrease of infected individuals followed by a subsequent rise in recoveries over time. This pattern underscores the complex challenge of managing and controlling infectious diseases within a population. Figure (10)(e) shows the comparative chaotic behaviors between recovered and pathogen individuals. In the context of COVID-19 in Thailand, the chaotic behavior of recovered and pathogen individuals is marked by a swift rise in the number of recoveries and infections, followed by a gradual decline. This pattern mirrors the dynamic nature of disease transmission and the influence of public health interventions in managing the epidemic. The chaotic behavior of the different compartments in the feasible region for a stable solution in the domain is shown in Figure (11) which represents the complete relation of the compartment and the memory effect of the fractional operator to stabilize the solution in the bounded region. The fractal-fractional operators are thus superior tools for investigating the more complicated behavior of the proposed system. These variables interact in intricate ways that can be challenging to represent using conventional modeling techniques. The intricate relationships between these variables and how they affect the spread of disease are better understood by using chaos figures. It is evident that the dynamics of the model's several compartments have changed in response to shifting fractional or fractal orders. The figures (8)-(11) show the orbit trajectories. Limit cycle behaviors of the model. It's interesting to note that while the equilibrium points are consistent, in both the order and integer order models the solution of the fractional order model gradually converges to the fixed point over a period. We have also explored attractors, which pose challenges to both fractional order operators in reproducing complex behaviors and stable solutions within a feasible domain.

This method offers an understanding of how population dynamics evolve over time enabling accurate predictions and analysis. Additionally, it offers an insight into how fractal geometry and fractional calculus interact in modeling. By illustrating the dynamics of disease transmission this approach can aid in developing treatment and prevention strategies. Furthermore, combining fractal geometry with calculus enhances our comprehension of the underlying mechanisms governing population dynamics. It also creates opportunities to explore the relationships between systems and mathematical modeling. The incorporation of fractal derivatives empowers researchers to forecast and study disease transmission within populations, with accuracy.

9 Conclusion

The SQEIRP model's results, which predict a high number of hospitalized and infected cases within a short period following infection commencement, demonstrate the outbreak's potential severity. Using the numerical technique, we were able to analyze data from the literature and come up with some really interesting results for different fractional orders that help counteract the negative effects of COVID-19 on society and support theoretical observations. The development of the SQEIRP model with the integration of the non-singular kernel of the Mittag-Leffler Law represents a significant stride towards tailoring mathematical frameworks to suit the unique lifestyle and epidemiological characteristics of the Thai population during the COVID-19 epidemic. The proposed model satisfied the biological feasibility criteria such as unique solution, uniqueness, existence and uniqueness, and Ulam-Hyers stability. Sensitivity analysis reveals that the parameters β^{υ} and κ^{υ} significantly influence the basic reproduction number $\mathscr{R}_0$. The outcome attained from the SQEIRP model emphasizes the seriousness of the outbreak, forecasting a considerable number of infected and hospitalized cases shortly after infection onset. This highlights the crucial need for proactive measures to reduce the rise of COVID-19 cases beyond controllable levels. By integrating the non-singular kernel of the Mittag-Leffler Law, the model is capable of making more accurate predictions by accounting for sequential dependencies and memory effects inherent in epidemic developments. This improvement not only makes the model better at predicting the spread of COVID-19, but it also offers the public and policymakers insightful information that they can use to put effective preventive measures in place. Subsequent investigations may concentrate on using sophisticated analytical methods to augment the prognostic potential and pragmatic uses of epidemic models. Optimal control theory can also be used to investigate optimal solutions for our scenario.

Acknowledgements This study was supported by the Scientific Research Project for High-Level Talents of Youjiang Medical University for Nationalities, Baise, Guangxi, China under grant number yy2023rcky002.

Author Contributions Saba Jamil: Analysis, Methodology, Writing-original draft. Parvaiz Ahmad Naik: Conceptualization, Analysis, Funding acquisition, Supervision, Review & editing. Muhammad Farman: Analysis, Investigation, Methodology, Writing-original draft. Muhammad Umer Saleem: Software, Validation, Numerical simulations, Review & editing. Abdul Hamid Ganie: Resources, Review & editing.

Data Availability The data supporting this study's findings are available within the article.

Declarations

Conflict of interest None declare.

References

1. Thompson, H.A., Mousa, A., Dighe, A., et al.: Severe acute respiratory syndrome coronavirus 2 (SARS-CoV-2) setting-specific transmission rates: a systematic review and meta-analysis. Clin. Infect. Dis. **73**, e754–e764 (2021)
2. Algehyne, E.A., Din, R.: On global dynamics of COVID-19 by using SQIR type model under non-linear saturated incidence rate. Alex. Eng. J. **60**, 393–399 (2021)
3. Hafeez, A., Ahmad, S., Siddqui, S.A., et al.: A review of COVID-19 (Coronavirus Disease-2019) diagnosis, treatments and prevention. Ejmo. **4**, 116–125 (2020)
4. Aljadeed, R., AlRuthia, Y., Balkhi, B., et al.: The impact of COVID-19 on essential medicines and personal protective equipment availability and prices in Saudi Arabia. Healthcare **9**, 290 (2019)
5. WHO, E.: World Health Organization (WHO) Coronavirus (COVID-19) Dashboard. Who. int. (2022)
6. TunÃ, C., Golmankhaneh, A.K., Branch, U.: On stability of a class of second alpha-order fractal differential equations. AIMS. Math. **5**, 2126–2142 (2020)
7. Atangana, A.: Modelling the spread of COVID-19 with new fractal-fractional operators: can the lockdown save mankind before vaccination. Chaos Soliton Fractal **136**, 109860 (2020)
8. Jitsinchayakul, S., Humphries, U.W., Khan, A.: The SQEIRP mathematical model for the COVID-19 epidemic in Thailand. Axioms **12**, 75 (2023)
9. Yavuz, M., Boulaasair, L., Bouzahir, H., et al.: The impact of two independent Gaussian white noises on the behavior of a stochastic epidemic model. J. Appl. Math. Comput. Mech. **23**(1), 121–134 (2024)
10. Abidemi, A., Owolabi, K.M.: Unravelling the dynamics of lassa fever transmission with nosocomial infections via non-fractional and fractional mathematical models. Eur. Phys. J. Plus **139**, 108 (2024)
11. Joshi, H., Yavuz, M., Townley, S., Jha, B.K.: Stability analysis of a non-singular fractional-order COVID-19 model with nonlinear incidence and treatment rate stability. Phys. Scr. **98**, 045216 (2023)
12. Naim, M., Sabbar, Y., Zeb, A.: Stability characterization of a fractional-order viral system with the non-cytolytic immune assumption. Math. Model. Numer. Simul. Appl. **2**(3), 164–176 (2022)
13. Owolabi, K.M.: Computational study for the Caputo sub-diffusive and Riesz super-diffusive processes with a fractional order reaction-diffusion equation. Partial Differ. Equ. Appl. Math. **8**, 100564 (2023)
14. Rihan, F.A.: Delay Differential Equations and Applications to Biology. Springer (2021)
15. Tajadodi, H., Khan, A., Gómez-Aguilar, J.F., et al.: Optimal control problems with Atangana-Baleanu fractional derivative. Optim. Contr. Appl. Met. **42**, 96–109 (2021)
16. Kouidere, A., Youssoufi, L.E., Ferjouchia, H., et al.: Optimal control of mathematical modeling of the spread of the COVID-19 pandemic with highlighting the negative impact of quarantine on diabetics people with cost-effectiveness. Chaos Soliton Fractal **145**, 110777 (2021)
17. Ullah, R., Waseem, M., Rosli, N.B., et al.: Analysis of COVID-19 fractional model pertaining to the Atangana-Baleanu-Caputo fractional derivatives. J. Funct. Spaces **2021**, 2643572 (2021)
18. Joshi, H., Jha, B.K., Yavuz, M.: Modelling and analysis of fractional-order vaccination model for control of COVID-19 outbreak using real data. Math. Biosci. Eng. **20**(1), 213–240 (2022)
19. Naik, P.A., Yavuz, M., Qureshi, S., Zu, J., Townley, S.: Modeling and analysis of COVID-19 epidemics with treatment in fractional derivatives using real data from Pakistan. Eur. Phys. J Plus **135**(10), 795 (2020)

20. Das, M., Samanta, G.: Stability analysis of a fractional ordered COVID-19 model. Comput. Math. Biophys. **9**, 22–45 (2021)
21. Baba, I.A., Nasidi, B.A.: Fractional order model for the role of mild cases in the transmission of COVID-19. Chaos Soliton. Fractal **142**, 110374 (2021)
22. Farman, M., Besbes, H., Nisar, K.S., et al.: Analysis and dynamical transmission of COVID-19 model by using Caputo-Fabrizio derivative. Alex. Eng. J. **66**, 597–606 (2023)
23. Ma, W., Ma, N., Dai, C., et al.: Fractional modeling and Optimal Control Strategies for Mutated COVID-19 Pandemic. Math. Methods Appl, Sci (2022)
24. Khan, H., Alzabut, J., Shah, A., et al.: On fractal-fractional waterborne disease model: a study on theoretical and numerical aspects of solutions via simulations. Fractal **31**(4), 2340055 (2023)
25. Selvam, A., Sabarinathan, S., Noeiaghdam, S., et al.: Fractional fourier transform and Ulam stability of fractional differential equation with fractional Caputo-type derivative. J. Funct. Spaces **2022**, 1–5 (2022)
26. Aslam, M., Murtaza, R., Abdeljawad, T., et al.: A fractional order HIV/AIDS epidemic model with Mittag-Leffler kernel. Adv. Differ. Equ. **2021**, 1–15 (2021)
27. Farman, M., Amin, M., Akgul, A., et al.: Fractal-fractional operator for COVID-19 (Omicron) variant outbreak with analysis and modeling. Res. Phys. **39**, 105630 (2022)
28. Ma, N., Ma, W., Li, Z.: Multi-model selection and analysis for COVID-19. Fractal Fract. **5**(3), 120 (2021)
29. Ma, W., Zhao, Y., Guo, L., et al.: Qualitative and quantitative analysis of the COVID-19 pandemic by a two-side fractional-order compartmental model. ISA Trans. **124**, 144–156 (2022)
30. Xu, C., Pang, Y., Liu, Z., et al.: Insights into COVID-19 stochastic modelling with effects of various transmission rates: simulations with real statistical data from UK, Australia, Spain, and India. Phys. Scr. **99**, 025218 (2024)
31. Xu, C., Dan, M., Zixin, L., et al.: Bifurcation dynamics and control mechanism of a fractional-order delayed Brusselator chemical reaction model. MATCH Commun. Math. Comput. Chem. **89**(1), 73–106 (2023)
32. Rihan, F.A., Udhayakumar, K., Sottocornola, N., et al.: Stability and bifurcation analysis of the Caputo fractional-order asymptomatic COVID-19 model with multiple time-delays. Int. J. Bifur. Chaos **33**, 2350022 (2023)
33. Rihan, F.A., Gandhi, V.: Dynamics and sensitivity of fractional-order delay differential model for coronavirus (COVID-19) infection. Prog. Fract. Differ. Appl. **7**(1), 43–61 (2021)
34. Padmavathi, T., Senthamilselvi, S., Santra, S.S., Govindan, V., Altanji, M., Noeiaghdam, S.: Rotational reaction over infected COVID-19 on human respiratory tract in the presence of soret effect with hall current. Bull. Irkutsk State Univ. Ser. Math. **40**, 15–33 (2022)
35. Sivashankar, S., Sabarinathan, S., Govindan, V., Fernandez-Gamiz, U., Noeiaghdam, S.: Stability analysis of COVID-19 outbreak using Caputo-Fabrizio fractional differential equation. Aims Math. **8**(2), 2720–2735 (2023)
36. Hedayati, M., Ezzati, R., Noeiaghdam, S.: New procedures of a fractional order model of novel coronavirus (COVID-19) outbreak via wavelets method. Axioms **10**(2), 122 (2021)